Hinterland environments of the Late Jurassic northern Weald Basin, England

Dinfa Vincent Barshep[1, 2] Richard Henry Worden[2]

[1]University of Liverpool, Department of Earth Ocean and Ecological Sciences, L69 3GP, United Kingdom, CGG services (UK) Limited, Tyn Y Coed, Pentywyn Rd, Llanrhos, Llandudno LL30 1SA, dinfabarshep@yahoo.co.uk, dinfa.barshep@cgg.com.

[2]University of Liverpool, Department of Earth Ocean and Ecological Sciences, L69 3GP, United Kingdom, (r.worden@liverpool.ac.uk)

ABSTRACT

Reconstructing provenance in sandstones can be challenging, especially when the hinterland palaeogeology is unknown due to burial, diagenesis or weathering of the original outcrops. As sedimentary processes alter the distribution of minerals in the depositional environment, the use of multiple provenance methods reduces uncertainties, because, together, they can account for depositionally-controlled textural and mineralogical re-distribution in a basin,. Here, we have applied petrography, X-ray fluorescence geochemistry and sedimentology to understand the provenance of shallow marine Corallian sandstones, with the aim of deducing the palaeogeology, palaeoenvironment and sediment distribution within the northern parts of the Upper Jurassic Weald Basin, onshore UK. The Corallian sandstones had a mixed mafic-felsic (intermediate), metasedimentary recycled orogen source. The hinterland experienced significant physical and chemical weathering under humid conditions. Corallian sandstones were relatively more chemically mature up-dip and more texturally mature down-dip. Chemically unstable grains and heavy minerals were relatively concentrated down-dip. Heterogeneous, sedimentologically-controlled mineral distribution patterns highlight potential errors which may be made in deriving source-area maturity. This study is significant as it illustrates the combined roles of provenance and deposition in controlling primary mineral distribution that then influenced the style of burial diagenesis. The work presented here emphasises the importance of a multi-proxy approach to improve provenance analysis.

Key words: Corallian sandstones, palaeoclimate, palaeogeology, provenance, sandstone geochemistry, Upper Oxfordian, Weald Basin

Correspondence

Richard Henry Worden, University of Liverpool, Department of Earth Ocean and Ecological Sciences, L69 3GP, UK. Email: r.worden@liverpool.ac.uk

1 INTRODUCTION

In ancient sandstones, direct evidence for palaeoenvironmental conditions in the sediment source-area are typically scarce and hence are commonly inferred, for example from the characteristics of sediment from surrounding basins (Sladen & Batten, 1984). Sandstone mineralogy and textural maturity are functions of their hinterland mineralogy, the dispersal paths that link the hinterland to the depositional basin, climate, and the sedimentary processes within the depositional basin (Dickinson & Suczek, 1979; Griffiths et al., 2019; Pettijohn, Potter, & Siever, 1973; Potter, 1978; Tobin & Schwarzer, 2013). It therefore follows that understanding sandstone provenance will potentially unlock information about conditions in the source-area, especially when the palaeogeology cannot be directly studied due to continued hinterland outcrop weathering or burial diagenetic obliteration of primary sedimentary character (Dickinson, 1988; Odom, Doe, & Dott, 1976). Understanding sediment source-areas is important as it enhances knowledge of the palaeogeography of sediment's hinterland, as well as palaeocurrent and palaeoslope directions which helps prediction of sediment movement (Pettijohn et al., 1973). Provenance studies can be practically applied to problems including basin evolution and tectonics (Dickinson, 1985), climate and relief (Folk, 1980; Ruffell & Rawson, 1994), discrimination of sandstone petrofacies and source-areas (Ingersoll, 1990), as well as palaeo-drainage and sediment dispersal patterns (Lowe, Sylvester, & Enachescu, 2011). Other practical applications of provenance analysis recognise that sand with different framework grain compositions typically have different diagenetic pathways which can affect porosity during burial; hence provenance studies are applied in hydrocarbon exploration, mining and groundwater studies (Ärlebrand, Augustsson, Escalona, Grundvåg, & Marín, 2021; Boggs, 2009; Daneshvar & Worden, 2017; Dickinson & Suczek, 1979; Pettijohn et al., 1973; Tobin & Schwarzer, 2013; Worden, Armitage, et al., 2018).

Many provenance analysis studies have been undertaken using element geochemistry (Middelburg, van der Weijden, & Woittiez, 1988; Middleton, 1960; Nesbitt, Young, McLennan, & Keays, 1996; Potter, 1978) and detrital mineralogy (Basu, Young, Suttner, James, & Mack, 1975; Blatt, 1967; Dapples, Krumbein, & Sloss, 1953; Dickinson, 1985; Lowe et al., 2011; Nesbitt et al., 1996; Reinson, Bureau of Mineral Resources, & Geophysics, 2015) complemented by other techniques such as facies analysis, wireline log analysis, and palynology. Most studies have focused heavily on mineralogical and bulk geochemical analyses, for example, Nesbitt et al. (1996), Basu et al. (1975); Dickinson and Suczek (1979). Sedimentary processes, such as hydrologic sorting which can cause mineralogical as well as textural redistribution of sediment (Dokuz & Tanyolu, 2006; Kroonenberg, 1992), are typically overlooked in analysing provenance and source area evolution; it is significant that there have been few studies incorporating sedimentological processes within the depositional basin in provenance studies (Odom et al., 1976). This oversight may potentially lead to errors in provenance analysis because sedimentological processes continue to modify the sediment mineralogy derived from a source area (Odom et al., 1976). In this study we have applied mineralogical, geochemical, wireline and sedimentological analyses to investigate the provenance of the Weald Basin's Upper Jurassic Corallian sandstones. These techniques have been chosen to help determine the mineralogy, degree of weathering and the climate in the sediment source-area (Nesbitt et al., 1996; Pettijohn et al., 1973; Potter, 1978; Ruffell & Rawson, 1994). Sedimentological analysis have been used to deduce potential controls of sediment redistribution and mineralogical enrichment in the basin. Wireline logs have allowed an unbiased separation of sand-rich from clay-rich stratigraphic zones.

This study focused on the sand-rich portions of the Corallian sandstones, as defined by neutron-density cross-over plots, because precise identification of detrital components by point counting is best achieved in sand-grade sediments compared to mud-grade sediments (Dickinson, 1985). Data and samples have come from the Palmers Wood and Bletchingley petroleum accumulations in the northern margin of the Weald Basin, close to the London-Brabant Massif (LBM) (Figure 1a, 1c). The Corallian contains producible oil in these two accumulations and several wells have been cored, most wells have good quality downhole wireline log data. The LBM has been identified by several authors as the likely source-area for the Weald Basin (Butler & Pullan, 1990; Hawkes, Fraser, & Einchcomb, 1998; Sladen &

Batten, 1984) but the Oxfordian section and sediment supply to the Weald Basin have not been extensively studied. The Palmers Wood and Bletchingley fields are separated by a syn-sedimentary fault and seem to have subtly contrasting high and lower energy hydrodynamic regimes, sedimentology and sediment dispersal patterns updip and downdip of the fault (Barshep & Worden, 2022). The two fields are relatively close to the London-Brabant Massif (~ 15 km) (Figure 1). The Corallian (Oxfordian) sandstones are at shallow present-day depths (< 1000 m true vertical depth) and have not been buried deeper than about 1500 m, hence they are not significantly altered by mesodiagenesis (Barshep & Worden, 2021, 2022). The lack of burial diagenesis and relative proximity to the sediment source terrain make the case study suitable for the reconstruction of the palaeogeology, palaeoclimate and palaeotectonic setting of the Jurassic LBM area, as well as for the investigation of the effects of sedimentological controls on provenance analysis. Our objective is therefore to understand the palaeogeology, palaeoclimate and palaeotectonic setting of the Jurassic LBM area, as well as to investigate the effects of sedimentological controls on provenance analysis. To achieve this, the study will answer the following research questions:

(1) What was the source-area palaeogeology for the Corallian sandstones from the northern part of the Weald Basin?
(2) Is there evidence of source-area migration?
(3) What were the palaeoclimatic conditions in the Upper Jurassic in the source-area?
(4) What was the Upper Jurassic tectonic setting of the source-area?
(5) What are the effects of tectonism on sediment distribution?

2 GEOLOGICAL HISTORY AND SEDIMENT SOURCE

The Weald Basin, located in southeast England, is limited to the north by the London-Brabant Massif (LBM), the Hampshire-Wessex Basin, to the west and the Portsdown-Middleton trend, and to the south (Butler & Pullan, 1990; Hansen, Blundell, & Nielsen, 2002; Lake & Karner, 1987) (Figure 1). The geological history of the Weald Basin can be summarised into three phases (i) Palaeozoic deformation of basement rocks (ii) Early Jurassic to Lower Cretaceous basin subsidence and (iii) Cenozoic uplift.

The Palaeozoic deformation of basement rocks occurred during the Variscan (also known as the Hercynian) Orogeny (Hansen et al., 2002; Trueman, 2003) with resulting east-west trending compressional fault development (Figure 1). These faults evolved to become extensional faults resulting in the Mesozoic extensional basin due to thermal subsidence accompanied by block faulting (Butler & Pullan, 1990). Basin formation was accompanied by the Rhaetic transgression and the deposition of the White Lias, Lower Lias, Middle Lias and Upper Lias units in the Lower Jurassic (Figure 2) (Andrews, 2014; McLimans & Videtich, 1989; Sellwood, Scott, & Lunn, 1986). The Inferior Oolite and Great Oolite Formations were deposited in the Bajocian and Bathonian, respectively, on a carbonate platform formed due to uplift (Lake & Karner, 1987; Talbot, 1973). The Callovian to Lower Oxfordian saw continued rifting and deposition of the transgressive Oxford Clay Formation, Corallian Group, Kimmeridge Clay Formation and the Tithonian Portland sandstones (Figure 2). The sea level then fell causing the sabkha-type Purbeck Group sediments to be deposited at the end of the Jurassic through to the Lower Cretaceous (Butler & Pullan, 1990; Hansen et al., 2002; Radley, 2006). Deposition of the Purbeck Group was followed by Valanginian Wealden Group clastic sediments (Radley, 2006). It is likely that there was Chalk, Upper and Lower Greensand, and Palaeogene clastic sediment deposition, subsequently removed due to uplift and inversion of the E-W inherited Palaeozoic previously extensional faults.

Cenozoic uplift was caused by compressive forces from the south of the basin during the opening of the North Atlantic (Jones, 1999). This episode has been attributed to the Pyrenean Orogeny (Parrish, Parrish, & Lasalle, 2018), based on the dating of calcite veins. Cenozoic uplift caused erosion and removal of sediments younger than the Wealden Group (Sellwood, Scott, Mikkelsen, & Akroyd, 1985), including Chalk, Upper and Lower Greensand, and Palaeogene clastic sediments.

The main source-area for sediment in the Weald Basin was the London-Brabant Massif (LBM), also known as London Platform (Figure 1a, 1c) (Allen, 1975; Butler & Pullan, 1990; Hawkes et al., 1998; Sladen & Batten, 1984). Rocks from the LBM were weathered and sediments transported southward into the Weald Basin (Allen, 1975; Butler & Pullan, 1990; Hawkes et al., 1998; Sladen & Batten, 1984). The LBM consists of Precambrian crystalline basement and metasedimentary rocks, as well as Ordovician and Silurian volcanic and clastic sedimentary rocks (Rijkers, Duin, Dusar, & Langenaeker, 1993). The LBM is an east-west trending stable structure located beneath southeast England, extending across the southern North Sea and into Belgium (Pharaoh, 2018; Rijkers et al., 1993). In contrast to the Weald Basin to the south, the LBM did not subside in the Mesozoic, as it had minimal Variscan-induced internal structures, in contrast to the Weald Basin (Chadwick, 1985). The LBM thus remained as a structural high to the north of the Weald Basin and has been reported to be the primary sediment source for the Upper Jurassic Corallian sandstones (Hawkes et al., 1998).

3 MATERIALS AND METHODS

3.1 Core log analysis

High-resolution sedimentary core logging, recording cm- and mm-scale features, was undertaken on core from three wells, Bletchingley 5 (BL5), Palmers Wood 3 (PW3) and Palmers Wood 7 (PW7) at the British Geological Survey (BGS) core store, Keyworth, Nottinghamshire, UK. BL5 was drilled in 2008, PW3 was drilled in 1984 and PW7 was drilled in 1990. All depths were originally recorded in feet but have been converted to metres in this study. The cores were logged at a resolution of 1:24, recording grain size, lithology, sedimentary structures, and bioturbation. 56.1 ft (17.1 m) of core was logged from PW3, with 54.5 ft (16.6 m) from PW7 and 65 ft (19.8 m) from BL5. The detailed sedimentary logs were summarised and digitised to a scale of 1:240 for comparison to wireline log data. All reported depths are measured depths, as opposed to vertical depths, except where otherwise stated.

3.2 Wireline log and core analysis

A suite of modern conventional wireline logs was available for each well including caliper, gamma, compressional sonic, bulk density, neutron and deep and shallow resistivity logs. Wireline data were reported every 15 cm, as this reflects the minimum resolution of the suite of logging tools. Core analysis data were also available for each well, including porosity, permeability, and grain density data.

Neutron-density cross-over diagrams were plotted using Rstudio to define sand-rich areas, i.e., sand packages in the logs similar to pay zones in conventional petrophysical analysis (Tiab & Donaldson, 2012). Core to log depth shifts were corrected by optimising the match of both core porosity to density logs and the sedimentary log-determined presence of mudstones to gamma ray logs (Figure 3).

3.3 Handheld XRF analysis

One hundred and eighty-nine sample points were analysed from the sand packages in BL5, PW3 and PW7 using a Thermofisher Niton XL3T GOLDD (Geometrically Optimized Large Area Drift Detector) handheld X-ray fluorescence (XRF) device. The XRF sample points include 37 from PW7, 60 from BL5 and 27 from PW3. XRF analysis points were directly matched to core analysis plug points to allow XRF data to be related to core analysis data.

Before measurements, the handheld XRF was tested for precision by taking ten readings on the same sample point for a duration of 50 seconds, 100 seconds, 150 seconds and 200 seconds and the data compared for repeatability. Repeatability was calculated by comparing the standard deviations for all ten readings for silicon, iron, aluminium, calcium, zircon and titanium. The data showed the least deviations at ≥150 seconds analysis duration; consequently, a sampling time of 150 seconds was chosen for the whole core measurements to optimise precision and measurement duration. Forty-three elements were analysed although some readings, especially trace elements, below detection.

Data from XRF analyses were analysed using geochemical proxies for lithology, provenance, and weathering for clastic sediments. Table 1 summarises some useful proxies and their applications in the geochemical analysis of sediment.

3.4 Optical petrography

Optical microscopy and point counting were carried out on 51 polished sections from PW7, PW3 and BL5 using an Olympus BX51 transmitted light microscope. Analyses were undertaken to determine mineralogy, textural relationships and cement types. Thirty-three samples from the sand-rich zones were selected for point counting using an Olympus BX53M microscope aided by the Conwy Valley Systems Petrog software with samples mounted on a Petrog stage. The samples analysed include 18 polished sections from BL5, five from PW3, and ten from PW7. Three hundred points were analysed for each polished section using a x10 objective, for a statistically representative analysis of each polished section. Point counting focused on differentiating diagenetic minerals from detrital minerals with emphasis on polycrystalline and monocrystalline quartz, feldspars, lithic grains and cement types.

3.5 SEM analysis

A bench-top Hitachi TM3000 scanning electron microscope was used to undertake Back-Scattered Scanning Electron Microscopy (BSEM) at the University of Liverpool's Central Teaching Labs (CTL). The BSEM analysis was carried out to determine mineralogy, mineral/cement types and textural relationships.

3.6 SEM-EDS

Scanning electron microscope-energy dispersive spectroscopy (SEM-EDS) imaging and analysis was carried out for automated quantitative mineral analysis (Worden, Utley, et al., 2018). The SEM-EDS instrument used in this study was an FEI WellSite QEMSCAN, at the University of Liverpool, using a tungsten-filament, operating at 15 kV and equipped with two Bruker EDS detectors (Wooldridge, Worden, Griffiths, & Utley, 2018). The technique makes use of a Scanning Electron Microscope (SEM) equipped with two or more high speed Energy Dispersive X-Ray Spectroscopy (EDS) detectors (Armitage et al., 2011; Barshep & Worden, 2021; Worden & Utley, 2022; Worden, Utley, et al., 2018) to give a quantitative proportion of mineral assemblages. In this study, the ideal minimum practical spacing resolution of 2 µm was used for higher resolution analyses and 20 µm spacing was used where average mineralogy across a whole polished section was required. The identification and quantification of minerals was determined using a pre-defined mineral database, known as Species Identification Protocol (SIP) archived in a mineral library (Armitage et al., 2010; Pirrie, Butcher, Power, Gottlieb, & Miller, 2004). Each mineral was assigned a colour for identification and representation in images, and modal compositions were collated based on the areas each mineral occupied in the polished section.

QEMSCAN analysis produces a mineral map hence QEMSCAN analysis is included here to complement optical microscopy and petrography point counting in the identification of both detrital, and authigenic minerals as well as their textural relationships.

4 RESULTS

4.1 Core description and wireline

The Corallian clastic sediments are composed of sandstones and siltstones with intermittent argillaceous intervals (Figure 3). Sandstones represent the dominant lithology with siltstones and mudstones making up minor portions of the basal, mid and top parts of the Corallian clastic section (Figure 3). PW7 and PW3 are composed of medium-grained sands with minor fine-grained sand, silt and clay (Figure 3). BL5 is predominantly composed of medium-grained sand and upper fine-grained sand, with minor very fine–grained sand, silt and clay (Figure 3). The sandstones in all three wells have abundant sedimentary structures including low-angle cross-stratification, planar cross-stratification, trough cross-stratification, low-angle lamination, mud drapes, massive bedding, as well as hummocky cross-stratification. Other sedimentary structures include flaser bedding, lenticular bedding, wave ripple lamination, current ripple lamination, cross-lamination and climbing current ripple lamination (Figure 3). Planar cross-stratification (Figure 3a at 1131.4 m), hummocky cross-stratification (Figure 3a at 1123.4 m) and trough-cross-stratification (Figure 3b at 1085.4) are more common in PW3 and PW7; in contrast flaser beds (Figure 3c at 2206.8 m), mud drapes (Figure 3c at 2196.9) and argillaceous intervals mottled by bioturbation (Figure 3c at 2207.4 m) are more common in BL5.

To objectively delineate sand-rich, from clay-rich, intervals, neutron-density cross-over plots (Rider, 1986) were used in conjunction with the sedimentary logs (Figure 3), leading to the identification of seven sand packages. These are labelled PW7-1, PW7-2, PW3-1, PW3-2, BL5-1, BL5-2 and BL5-3; all are separated by argillaceous layers (Figure 3). The sand packages have been correlated across the three wells. PW7-1, PW3-1 and BL5-1 can be easily correlated across all wells. Similarly, PW7-2, PW3-2 and BL5-2 can be correlated across all wells (Figure 3). In contrast, BL5-3 cannot be correlated with any other sand package in the PW wells (Figure 3).

4.2 Geochemical analysis

To compare the composition of sediments in the various sand packages, we have used numerous element cross-plots as well as geochemical indices (Table 2). Indices and ratios tend to be better than element concentrations for studying clastic sediments as they remove the effects of variable dilution by dominant minerals such as calcite and quartz. Indices are preferred to ratios as they vary from 0 to 1 rather than from infinitely small to infinitely large values. Indices provide proxies for bulk lithology, mineralogy, and weathering characteristics and can complement other mineralogical analysis techniques (Table 2). The geochemical indices have been calculated using the parts per million (ppm) values of the elements being compared. Lines have been drawn on the cross-plots to indicate the range for granite and basalt (Figure 4a-4e) thus revealing mafic and felsic provenance, using end-member values reported in Krauskopf (1979).

Ti and Al were compared as they are proxies for mafic or felsic provenance respectively (Andersson & Worden, 2004). A cross-plot of Ti and Al indicates a maximum Ti atomic fraction below 0.07 and aluminium has an atomic fraction of up to 0.9 (Figure 4a). The sample points plot predominantly between the trajectories for basalt and granite suggesting a mixed mafic-felsic (intermediate) provenance for the Corallian sandstones (Figure 4a).

The distribution of Ti to Al in the sand packages does not show a systematic pattern and suggest a general intermediate origin for the Corallian sandstones (Figure 5e). Sample points however cluster around the origin of Figure 4a confirming a high degree of quartz enrichment (as the Ti and Al are highly diluted) in these compositionally intermediate rocks.

The cross-plot of Si versus Al (Figure 4b), as well as the Si to Al index (Figure 5a), indicate a high proportion of Si relative to Al suggesting that quartz is vastly dominant over feldspars, micas, or other clay minerals which contain Al. The sample points plot closer to the Si axis and away from the basalt and granite lines suggesting significant quartz enrichment by secondary processes, such as weathering and hydrologic sorting (Kroonenberg, 1992).

The cross-plot of K versus Al (Figure 4c) confirms the enrichment of Si (note the concentration of samples near the origin) and also indicates the enrichment of Al relative to K because Al has an atomic fraction of up to 0.85 while K has a maximum atomic fraction less than 0.3. A significant proportion of samples plot along the granite line suggesting the presence of felsic minerals common in granites such as K-feldspar, and muscovite. The K versus Al plot approximates the chemical index of alteration (CIA) of Nesbitt and Young (1982) where the relatively insoluble Al is compared with the sum of oxides of Al plus relatively soluble Na, K, and Ca. The Al to K index (Figure 5b) indicates intense weathering with mean values greater than 0.5. Sand packages BL5-1, 2 and 3 have lower mean values compared to the Palmers Wood sand packages.

Fe is present in significant quantities in these rocks (Figure 4d); the Fe-Al relationship suggests the presence of Fe-rich alumino-silicates, such as berthierine or biotite. A significant proportion of samples plot away from the granite and basalt lines, closer to the Fe axis suggesting enrichment by processes different to simply being sourced from basalt versus granite (Figure 4d). Fe is not enriched in specific sand packages and there is no suggestion of different Fe source-areas (Figure 5d). Fe could have been transported to the depositional environment via Fe-rich minerals such as Fe-clay, and biotite, as indicated in the elevated Fe atomic fractions compared to Ti atomic fractions in (Figure 4e). Titanium could have been transported in the form of rutile, ilmenite, biotite or muscovite.

Rb versus Zr has been used as a geochemical weathering indicator as both are present in sediments and have different stability. Rubidium typically occurs in K-feldspar which is relatively unstable during weathering, while Zr occurs in zircon, which is a stable mineral during weathering (Everett et al., 2019). The cross plot of Rb versus Zr shows that the Corallian sandstones are depleted in Rb relative to Zr indicating significant weathering (Figure 4f). BL5-3 has an elevated Rb content suggesting elevated feldspar input and less intense weathering of the sediment source material (Figure 4f, Table 2). Boxplots of Zr-Rb index also indicate slightly elevated Zr in BL5-1 and 2 as well as PW7-1 and PW7-2 (Figure 5c) indicating elevated weathering in these sandstones.

4.3 Optical mineralogy

4.3.1 Detrital mineralogy

The Corallian sandstone packages are composed of fine- to medium-grained, predominantly moderately- to moderately-well-sorted sands with local poorly sorted sand intervals (Figures 6, 8; Table 3). The detrital components of the Corallian sandstones include monocrystalline quartz, polycrystalline quartz, K-feldspar, plagioclase feldspar, Fe-ooids and bioclasts (Figures 6, 8).

Monocrystalline quartz is present as rounded to sub-rounded grains (Figure 6a), which locally show undulose extinction under cross-polarised light (Figure 6a). Polycrystalline quartz is present as angular to sub-rounded grains (Figure 6a) and is recognised under cross-polarised light as a single grain composed of several interlocking crystals each of which has distinct undulose extinction under cross-polarised light (Figure 6a). Quartz grains have embayments filled by early calcite (Figure 6a) which suggests pre-diagenetic or early diagenetic corrosion and embayment.

K-feldspar and plagioclase feldspars are present in small quantities as angular grains in both the coarser-grained as well as finer-grained samples (Figures 7, 8). The K-feldspar grains occur as both altered and unaltered grains (Figure 6a, 8a). Feldspars are more abundant in the fine-grained sand- to clay-size-fractions (Figure 6c, 6d, 7c, 7d).

Fe-ooids occur as detrital grains with cement aligned along their outer grain boundaries (Figure 8b). Other minor detrital grains include biotite, illite, kaolinite, glauconite, rutile, apatite, and muscovite (Figures 6, 8) as well as zircon, and ilmenite.

Detrital matrix occurs locally (Figures 6c,6d,7c,7d) with compositions ranging from siderite matrix (Figures 6c, 7b) to a mixture of fine-grained minerals of unresolvable mineralogy under an optical microscope (Figure 6d). QEMSCAN analysis however shows a detrital matrix mineralogy of illite, muscovite, biotite, K-feldspar, plagioclase feldspar, rutile, quartz, kaolinite, and glauconite (Figures 7c, 7d).

The average total quartz (Qt), feldspar (F) and lithic grain (L) compositions of the sandstones are typical of quartz arenites with average composition $Qt_{97.2}F_{2.3}L_{0.6}$ (Figure 8a). The average proportion of monocrystalline quartz (Qm), feldspar (F) and lithic grains plus polycrystalline quartz (Lt) is $Qm_{76.5}F_{2.3}Lt_{21.2}$, typical of a quartzose recycled orogen after Dickinson (1985) (Figure 8b) where sediments are recycled and transported from deformed uplands, such as fold-thrust systems. BL5 has more monocrystalline quartz and plots closer to the craton interior orogen than PW3 and PW7 (Figure 9b). The monocrystalline quartz is more abundant in the BL5 sandstones with sand packages BL5-1 and BL5-3 having the greatest abundances (Figure 10b).

BL5 has a slightly higher feldspar content than the other wells, especially in sandstone package BL5-3, which plots closer to the craton interior orogen (Figure 9b). The lithic grain fragments are dominantly of metamorphic origin (Figure 9c) with minor sedimentary lithic grains and no igneous grains present (Figure 9c). Polycrystalline quartz comprises an average of about 16.1% with minor extrabasinal chert, extrabasinal quartzite, extrabasinal mudstone, and extrabasinal sandstone making up less than 2% of total rock volume (Table 3). Polycrystalline quartz is more abundant in the Palmers Wood sand packages PW7-2, PW3-1, PW7-1 and PW3-2 (in order of abundance) and less abundant in BL5-1, BL5-3 and BL5-2, in order of abundance (Figure 10c).

Grain size analysis indicates that the Palmers Wood sand packages have coarser grain sizes than the Bletchingley sand packages (Figure 10a). This systematic difference in grain size suggests different processes were responsible for deposition of sandstones in the two fields.

SEM-EDS boxplots analysis confirms the high quartz content of ≥ 90% of the detrital grains in all the sand packages (Figure 11a). SEM-EDS analysis also confirms elevated quantities of K-feldspar, plagioclase feldspar, zircon, rutile, illite, muscovite, biotite, Fe-clay and kaolinite in BL5 relative to the Palmers Wood sandstones (Figure 11). Illite, muscovite and biotite show a similar relationship by sand packages. SEM-EDS analysis shows the highest K-feldspar contents occur in BL5-2 and BL5-3 (Figure 11b) and the highest plagioclase feldspar contents occur in BL5-1, BL5-2 and BL5-3 (Figure11c).

4.3.2 Authigenic mineralogy

Authigenic mineral volumes were determined by optical point counting (Table 3). The dominant authigenic minerals in the Corallian sandstones include calcite, siderite, Fe-clay, pyrite, dolomite, authigenic illite and kaolinite. Other authigenic minerals include traces of quartz cement, and authigenic apatite (Figures 6, 8 andTable 4). Calcite is the main authigenic mineral in these sandstones, comprising up to 62%, with an average of 28.7%, of total rock volume (Table 4). Calcite fills intergranular and moldic pore spaces and separates detrital grains from each other; this suggests an early diagenetic origin (Figures 6a, 6b, 7a) (Barshep & Worden, 2021, 2022). Calcite cement is present at different stages of neomorphism of primary bivalve shells (Figure 6b); the outline of the bivalve shells is locally preserved by micrite envelopes.

The other cements include dolomite, with an average of 1.6% but up to 17.7%, siderite, with an average of 1.3% but up to 5.0% Fe-clay, with an average of 0.9% but up to 3.6% and pyrite, with an average of 0.6% but up to 2.7% (Table 4). Other cements include illite, with an average of 2.4% but up to 22.3%, quartz, with an average of 0.6% but up to 7.9% and kaolinite, with an average of 0.09% but up to 1.0 %.

Some close spatial relationships can be inferred between detrital and authigenic minerals; for example, authigenic berthierine occurs in close association with detrital biotite (Figure 7b). Also observed, is the presence of elevated quantities of calcite cement in bioclast-rich sections (Figures 6a, 6b,7a) and much less calcite cement in less bioclast-rich sections (Figures 6c and 6d).

5 DISCUSSION

5.1 Provenance

The QmFL composition of the Corallian sandstones within the quartzose recycled orogen (Figure 9b) suggests a provenance of stratified rocks that were deformed, uplifted and eroded (Dickinson, 1985; Dickinson & Suczek, 1979). Sediments from a recycled orogen are susceptible to significant reworking and can be from different sources (Dickinson, 1985, 1988). The medium-grained, monocrystalline quartz grains found in these sediments (Table 3, Figures 6a, 9b) indicate a primary plutonic igneous or metamorphic source-area (Pettijohn et al., 1973). The sediment maturity observed in the Corallian sandstones (Figure 9a, 9b) however is not necessarily typical of the relatively short transport distance (~15 km from the LBM to the study area) for plutonic rocks as such high maturity typically results from intense weathering, significant (100s to 1000s of km) transport ((Damuth & Fairbridge, 1970), or sediment recycling (Kroonenberg, 1992; Milliman, Summerhayes, & Barretto, 1975; Pettijohn et al., 1973; Potter, 1978; Tucker, 1981). Primary plutonic rocks would require significant alteration and hydrologic sorting to reach the level of maturity observed in the Corallian sandstones. Hydrologic sorting typically causes separation of grain size classes of specific minerals, sorting of minerals by density and enrichment in quartz content (Kroonenberg, 1992). Evidence for hydrologic sorting in the Corallian sandstones include significant quartz enrichment (Figures 4a-4f, 9a), elevated heavy minerals including zircon and rutile in BL5 (Figure 11d, 11e), elevated micas in BL5, separation of coarser-grained fractions and finer-grained fractions between the Palmers Wood area and Bletchingley area (Figure 10a), and concentration of feldspars in the Bletchingley area (Figure 11b, 11c).

Lithic grains, such as polycrystalline quartz and minor quartzite rock fragments, present in the Corallian sandstones (Figures 6a, 9c, 10c and Table 3) are indicative of metamorphic rocks in the source-area (Basu et al., 1975; Blatt, 1967; Pettijohn et al., 1973). Polycrystalline quartz is susceptible to mechanical weathering and typically disintegrates into monocrystalline quartz in mature sediments (Basu et al., 1975; Dickinson, 1985), hence polycrystalline quartz content is expected to be relatively low in mature sediments (Pettijohn et al., 1973). The high polycrystalline quartz content (up to 16%) in the mature Corallian sandstones suggests a much higher original polycrystalline quartz fraction, hence a significant metamorphic influence on provenance. The presence of lithic grains of sedimentary and metamorphic origin in the Corallian sandstones (Table 3) implies reworking of sedimentary or metamorphic rocks (Dickinson & Suczek, 1979). Given the evidence for sedimentary and metamorphic input, as well as sediment recycling and the absence of igneous grains (Figure 9c), the Corallian sediments were thus most likely sourced from a metasedimentary source-area.

The Ti-Al cross-plot has most sample points between the granite and basalt trajectories indicating a predominant mixed mafic-felsic provenance (Figure 4a), which includes metamorphosed equivalents of primary mafic and felsic rocks. Ti and Al are useful indicators of mafic and felsic provenance (Andersson & Worden, 2004) as Ti is enriched in basaltic rocks and Al is enriched in felsic rocks (Bhattacharjee & Mondal, 2021; Krauskopf, 1979). Ti and Al are both relatively stable and immobile elements under conditions of weathering and transport, hence are useful indicators of provenance in sediments (Hallberg, 1984). The distribution of Ti versus Al does not show a specific pattern by sand packages (Figure 5e) and predominantly plot within the intermediate provenance to indicate a general intermediate provenance for all the sand packages.

Elevated iron concentration in these sandstones relative to Al implies a significant iron input from Fe-Al minerals such as biotite and berthierine (Figures 4d, 5d). In sedimentary rocks, Fe-Ti minerals such as ilmenite tend to become depleted in Fe during their alteration due to the oxidation of iron in ilmenite (Morad & Adin, 1986). The elevated Fe in the Corallian sandstones indicates that Fe-rich minerals predominate over Ti-rich minerals in the source-area (Figure 4e) such that sedimentary oxidation did not significantly elevate the concentration of Ti relative to Fe. Iron was possibly sourced from primary crystalline rock or sediment pathways; the occurrence of Fe-rich minerals such as biotite (Figure 11h) strongly suggest an iron-rich hinterland. Many sample points plot away from the granite and basalt trajectories, close to the Fe-axis and near the origin of Figure 4d, suggesting that Fe was concentrated by secondary processes that have dominated the signal from the source-area. Berthierine ooids are Fe-rich minerals of sedimentary origin, and their occurrence in the Corallian sandstones (Figure 8b), possibly implies sedimentological concentration of Fe. The presence of diagenetic Fe-minerals, such as pyrite, siderite and dolomite, also suggests significant diagenetic concentration of Fe in the Corallian sandstones.

5.2 Tectonic settings

The average $Qm_{76.5}F_{2.3}L_{21.2}$ composition of the Corallian sandstones is indicative of a recycled orogen, for example where a fold and thrust belt has supplied the sediment. This is consistent with the history of the London Brabant Massif (LBM). The LBM is composed of Proterozoic to early Palaeozoic crystalline basement (Rijkers et al., 1993). These rocks are broadly similar to outcropping folded and faulted metasedimentary rocks in north-western England, including the Silurian Windermere Super Group. These are now dominated by low-grade metamorphosed clastic sediments (Kneller, Scott, Soper, Johnson, & Allen, 1994; Moseley, 1978). The LBM was deformed and metamorphosed during the Silurian Caledonian Orogeny (about 420 Ma.) (And possibly earlier). The interpretation of recycled sedimentary succession (in this case, probably metasediments) is consistent with the Corallian sandstones in the Weald Basin as they are composed mainly of recycled orogenic metasediments (Figure 9a, 9c).

Sediments from BL5 show more monocrystalline quartz than PW3 and PW7 and cluster closer to the craton interior orogen boundary (Figure 9b) which may indicate subtly different sources of sediment. The stratigraphically youngest sand package in BL5, BL5-3, has more feldspars

(Table 2) than all the other sand packages and clusters closest to the craton interior orogeny on the provenance diagram (Figure 9b). BL5-3 was deposited during a period of accelerated fault movement (Barshep & Worden, 2022). The higher feldspar content in BL5-3 is therefore probably the result of increased subsidence, which resulted in a steeper gradient thereby increasing erosion rates and sediment supply, leaving less time for feldspar alteration (Leeder, Harris, & Kirkby, 1998; Mack, 2003).

5.3 Climate and weathering

Mineralogical proxies in the Corallian sandstones at BL5, PW3 and PW7 suggest warm, humid, conditions in the sediment's hinterland with high precipitation rates and abundant fluvial recharge. These mineralogical proxies include (i) detrital kaolinite (Figure 7c,7d), (ii) iron-rich minerals including pyrite, Fe-dolomite, siderite and berthierine (Figures 6a, 6b, 7c, 7a, 7b), (iii) the dominance of quartz over feldspars (Figures 4a, 9a) (iv) embayed quartz grains (Figure 6b, 6c).

Kaolinite is indicative of warm tropical to sub-tropical climates with high rainfall rates and vegetation (Burley & Worden, 2003). This is because, the decay of organic matter under humid conditions creates acidity that enhances chemical weathering of alumino-silicate minerals to produce kaolinite (Burley & Worden, 2003; Hallam, 1975). The presence of kaolinite in detrital clay, the near absence of smectite and lack of evaporite minerals, such as gypsum/anhydrite (Figures 6,7,8), indicates humid conditions in the Upper Jurassic hinterland (Barshep & Worden, 2022).

Fe-dolomite, siderite, pyrite and berthierine in marine sediment typically indicates warm, humid, continental weathering as development of these iron-rich minerals in shallow marine environments involves terrigenous weathering under humid conditions to form lateritic soils, which, when eroded, transports iron into the marine environment (Hallam, 1984; Odin, 1988; Tucker, 1981; Worden et al., 2020).

The intense chemical weathering and iron enrichment in the source-area is emphasised by the low value of the K/Al index (Figures 4c, 5b), as enrichment of aluminium is typical of intense chemical weathering (Krissek & Kyle, 2001; Middleton, 1960). Other indicators of intense weathering include the dominance of quartz over feldspars (Figure 9a), depletion of Rb to Zr (Figure 4f) and presence of altered K-feldspar (Figure 8a) (Damuth & Fairbridge, 1970; Dickinson, 1985; Milliman et al., 1975). Rb and Zr have different mobility during weathering with Zr (in zircon and sphene) relatively more stable compared to Rb (which resides as trace element in potassium bearing minerals such as K-feldspar and mica) (Everett et al., 2019). The elevated zircon and feldspar concentrations in BL5 compared to PW3 and PW7 suggests intense mechanical weathering which typically does not completely remove feldspars from sediments but causes reduction in feldspar grain-size (Odom et al., 1976). The mechanical stability of zircon also causes zircon enrichment during physical weathering (Hubert, 1962) thereby indicating intense mechanical weathering of sediments supplied to BL5.

Embayments and signs of corrosion of quartz grains (Figures 6b, 6c, 8c) have been interpreted as evidence for tropical and subtropical environments (Cleary & Conolly, 1971; Potter, 1978) as well as volcanic provenance (Folk, 1968). The sediments here do not have volcanic lithic grains (Figure 9c) and locally occur with rounded edges (Figure 6a, 6b, 7a, 7b,7d) typical of sedimentary transport (Potter, 1978) and precluding volcanic origin to embayments and corrosion. Embayments are therefore interpreted to be formed in sediments weathered in tropical to subtropical conditions.

5.4 Sediment reworking and redistribution

The Corallian sandstones reveal mineralogical and textural differences between the Bletchingley and Palmers Wood areas which suggest different tectonic influences, changes in source-area weathering characteristics (Dickinson, 1985) or changes in depositional processes (Odom et al., 1976). Hydrologic sorting during transportation and deposition of sediments may have significantly affected the distribution and texture of Corallian sandstones sediments in the study area. Compared to the Palmers Wood wells, BL5 has elevated K-feldspar (Figure 11b), plagioclase feldspar (Figure 11c), zircon (Figure 11d), rutile (Figure 11e), muscovite (Figure 11g), biotite (Figure 11h) Fe-clay (Figure 11i) and monocrystalline quartz (Figure 10b). BL5 also has smaller grain size (Figure 10a) and less polycrystalline quartz than PW7 and PW3 (Figure 10c). The two fields are separated by a fault with evident up-dip and down-dip differences in hydrodynamic conditions (Barshep & Worden, 2021, 2022). Sedimentary structures such as planar cross-stratification, hummocky cross-stratification, trough cross-stratification and stacked massive beds predominate up-dip in PW3 and PW7 (Figure 3a, 3b) and indicate deposition at relatively high energy conditions. Down-dip, relatively lower energy conditions prevailed in the Bletchingley area as evident from frequent bioturbated intervals and sedimentary structures such as mud drapes (Figure 3c) (Barshep & Worden, 2022). The textural and mineralogical differences across the fault are most likely due to the hydrodynamic differences that are capable of causing differences in sediment characteristics and distribution (Folk, 1956; Kroonenberg, 1992; Odom et al., 1976).

It is not uncommon for mature sandstones to have elevated feldspar content in their finer-grained fractions, as observed in BL5 (Odom et al., 1976), because feldspars are not destroyed when abraded during mechanical weathering but become finer-grained, hence maturity might be due to grain size and sorting rather than mineralogy or hinterland climates (Odom et al., 1976). In addition, fine-grained feldspars can be carried in suspension for long distances in large water bodies (Milliman et al., 1975). The high energy, nearshore setting of the Palmers Wood area was susceptible to intense mechanical sediment reworking, hence hydrological sorting would cause (i) deposition of coarser-grained fractions in the higher energy Palmers Wood area (Figure 10a) (ii) potential mechanical breakdown of feldspars to finer-grains which remain in suspension in the higher energy Palmers Wood area, hence lower feldspar content (Figure 11b, 11c) and (iii) less mica, detrital illite and kaolinite in the Palmers Wood area as they would remain in suspension under high energy conditions (Figure 11f to 11i). The larger grain sizes in the Palmers Wood area and elevated polycrystalline quartz content indicate intense chemical weathering, capable of retaining coarser-grained sizes, diminished feldspar content and retention of polycrystalline grains that did not mechanically disintegrate during transport (Potter, 1978). Conversely, finer-grained mechanically unstable grains such as feldspars could be transported in suspension and deposited under lower energy conditions in the Bletchingley area; this would increase the feldspar content (Figures 5b, 5c, 11b, 11c) as well as fine-grained mineral fractions present in detrital clay, e.g. illite, muscovite, biotite, and kaolinite (Figure 11f, 11g, 11h, 11j). Evidence of intense physical weathering in the Bletchingley sediments include elevated monocrystalline quartz (Figure 10b), zircon (Figure 11d) and rutile (Figure 11e). Zircon and rutile have a high resistance to weathering and unlike unstable minerals like feldspars can be relatively enriched especially in the fine-grained fractions of weathered, transported and recycled sediments (Carroll, 1953; Dokuz & Tanyolu, 2006; Hallberg, 1984; Hubert, 1962; Kroonenberg, 1992; Pettijohn et al., 1973). Their abundance in the finer-grained sediments in BL5 is thus attributed to intense recycling and sorting, e.g. Dokuz and Tanyolu (2006). The elevated zircon, rutile, K-feldspar, plagioclase feldspar, biotite, muscovite, monocrystalline quartz and finer-grained sizes in the Bletchingley area were therefore not caused by source-area evolution but hydrological sorting.

In summary, the comparison of geochemical mafic-felsic end-members to investigate provenance and hydrological sorting is novel and improves on results derived from petrographic analysis as well as highlights hydrologic sorting. The incorporation of sedimentological analysis in this study highlighted the importance of sedimentary processes which caused redistribution of sediments in the basin which would otherwise have been attributed to source area migration, hence a misinterpretation of the effects of provenance on sediment supply. This work shows that it is important that sedimentological processes are included in provenance analyses.

The study is necessarily limited by its geographic extent as it is based on the Bletchingley and Palmers Wood area in the northern part of the Weald Basin. The study is also limited by the lack of availability of heavy mineral data. However, results from this study have broad implications for identifying and separating the effect of sedimentary processes such as hydrologic sorting from provenance analysis. In addition, the application of geochemical mafic-felsic end-members can enhance the interpretation of sediment weathering and mineral enrichment by sedimentary processes. The approach applied here has wider implications for provenance analysis in any sedimentary basin where surface outcrops are not available for direct correlation with depositional mineralogy.

6 CONCLUSIONS

1. The Corallian sandstones from the Palmers Wood and Bletchingley oil fields in the Weald Basin are composed of recycled, coarse siliciclastic sands from a source-area with intermediate mineralogy.
2. Petrographic evidence shows major sediment input from a sedimentary as well as metamorphic source-area with no evidence of input from unmetamorphosed igneous.

This has led to the conclusion of a metasedimentary provenance for the Corallian sandstones.

3. A provenance model suggests that the Corallian sandstones were sourced from a quartzose, recycled orogen, in this case probably the Silurian metasediments of the London Brabant massif, to the north of the Weald Basin.
4. Paleoclimate indicators suggest a humid source-area, capable of chemically weathering feldspars, creating kaolinite and oxidising iron compounds. The humid climate produced sufficient rainfall, capable of transporting coarse siliciclastic to the basin. Iron was probably enriched through transport over Fe-rich fairways and concentrated in the basin by the early diagenetic development of Fe-rich minerals.
5. Spatial, compositional and textural differences in sediment distribution were caused by hydrodynamic sorting, not source-area change. Tectonic evolution caused changes in depositional energy and enhanced the effects of hydrodynamic sorting.
6. Integrating depositional controls into provenance analysis has here enhanced understanding of source-area geology, source-area migration, estimation of hinterland sediment maturity, and generally enhance results from bulk mineralogy and geochemical analysis.

ACKNOWLEDGEMENTS

We wish to thank the British Geological Survey at Keyworth, Nottinghamshire, for access to the Palmers Wood and Bletchingley cores. We thank staff from IGas for providing log and core data as well as well reports. We are also grateful to the Petroleum Technology Development Fund (PTDF) for funding this research. Petrographic analysis was carried out at the Diagenesis Research Group at the University of Liverpool and portable X-ray fluorescence spectrometry was also provided by the Central Teaching Labs (CTL) of the University of Liverpool. The QEMSCAN used in this study was loaned to Liverpool's Diagenesis Research Group by the FEI courtesy of Alan Butcher. Basin modelling was undertaken using BasinMod software with the license gifted to the Diagenesis Research Group by Platte River Associates. Thanks to James Utley of the Diagenesis Research Group for his help with QEMSCAN analyses during the course of this study.

REFERENCES

Allen, P. (1975). Wealden of the Weald: a new model. *Proceedings of the Geologists' Association*, *86*(4), 389-437. doi:https://doi.org/10.1016/S0016-7878(75)80057-5

Andersson, P., & Worden, R. (2004). Mudstones of the Tanqua Basin, South Africa: An analysis of lateral and stratigraphic variations within mudstones, and a comparison of mudstones within and between turbidite fans. *Sedimentology*, *51*, 479-502. doi:10.1111/j.1365-3091.2004.00633.x

Andrews, I. J. (2014). *The Jurassic shales of the Weald Basin: geology and shale oil and shale gas resource estimation*. London UK: British Geological Survey Retrieved from https://www.ogauthority.co.uk/media/2773/bgs_decc_jurassicwealdshale_study_2014_main_report.pdf.

Ärlebrand, A., Augustsson, C., Escalona, A., Grundvåg, S.-A., & Marín, D. (2021). Provenance, depositional setting and diagenesis as keys to reservoir quality of the Lower Cretaceous in the SW Barents Sea. *Marine and Petroleum Geology*, *132*, 105217. doi:https://doi.org/10.1016/j.marpetgeo.2021.105217

Armitage, P. J., Faulkner, D. R., Worden, R. H., Aplin, A. C., Butcher, A. R., & Iliffe, J. (2011). Experimental measurement of, and controls on, permeability and permeability anisotropy of caprocks from the CO2 storage project at the Krechba Field, Algeria. *Journal of Geophysical Research: Solid Earth*, *116*(B12).

Armitage, P. J., Worden, R. H., Faulkner, D. R., Aplin, A. C., Butcher, A. R., & Iliffe, J. (2010). Diagenetic and sedimentary controls on porosity in Lower Carboniferous fine-grained lithologies, Krechba field, Algeria: A petrological study of a caprock to a carbon capture site. *Marine and Petroleum Geology*, *27*(7), 1395-1410. doi:10.1016/j.marpetgeo.2010.03.018

Barshep, D. V., & Worden, R. H. (2021). Reservoir Quality of Upper Jurassic Corallian Sandstones, Weald Basin, UK. *Geosciences*, *11*(11), 446. doi: https://doi.org/10.3390/geosciences11110446

Barshep, D. V., & Worden, R. H. (2022). Reservoir quality and sedimentology in shallow marine sandstones: Interplay between sand accumulation and carbonate and clay minerals. *Marine and Petroleum Geology*, *135*, 105398. doi:https://doi.org/10.1016/j.marpetgeo.2021.105398

Basu, A., Young, S. W., Suttner, L. J., James, W. C., & Mack, G. H. (1975). Re-evaluation of the use of undulatory extinction and polycrystallinity in detrital quartz for provenance interpretation. *Journal of Sedimentary Research*, *45*(4), 873-882. doi:10.1306/212f6e6f-2b24-11d7-8648000102c1865d

Bhattacharjee, C., & Mondal, S. K. (2021). Geochemistry of Fe-Ti oxide and sulfide minerals in gabbroic rocks and magnetitite of the Archean Mayurbhanj mafic complex (eastern India): Magma fractionation, thermometry and oxygen fugacity of re-equilibration, and implications for Ni-Cu mineralization. *Ore Geology Reviews*, *131*, 104005. doi:https://doi.org/10.1016/j.oregeorev.2021.104005

Blatt, H. (1967). Original characteristics of clastic quartz grains. *Journal of Sedimentary Research*, *37*(2), 401-424. doi:10.1306/74d716e0-2b21-11d7-8648000102c1865d

Boggs, J., Sam. (2009). Provenance of siliciclastic sedimentary rocks. In J. S. Boggs (Ed.), *Petrology of Sedimentary Rocks* (2 ed., pp. 220-267). Cambridge: Cambridge University Press.

Brookfield, M. (1973). Palaeogeography of the upper Oxfordian and Lower Kimmeridgian (Jurassic) in Britain. *Palaeogeography, Palaeoclimatology, Palaeoecology, 14*(2), 137-167. doi:https://doi.org/10.1016/0031-0182(73)90009-6

Burley, S. D., & Worden, R. H. (2003). *Sandstone diagenesis. [electronic book] : recent and ancient*: Malden, MA ; Blackwell Publishing, 2003.

Butler, M., & Pullan, C. P. (1990). Tertiary structures and hydrocarbon entrapment in the Weald Basin of southern England. *Geological Society, London, Special Publications, 55*(1), 371-391. doi:10.1144/gsl.sp.1990.055.01.19

Carroll, D. (1953). Weatherability of zircon. *Journal of Sedimentary Research, 23*(2), 106-116. doi:10.1306/d4269562-2b26-11d7-8648000102c1865d

Chadwick, R. (1985). Permian, Mesozoic and Cenozoic structural evolution of England and Wales in relation to the principles of extension and inversion tectonics. In A. Whittaker (Ed.), *Atlas of onshore sedimentary basins in England and Wales: Post-Carboniferous tectonics and stratigraphy* (pp. 9-25). Glasgow: Blackie.

Cleary, W. J., & Conolly, J. R. (1971). Distribution and Genesis of Quartz in a Piedmont-Coastal Plain Environment. *GSA Bulletin, 82*(10), 2755-2766. doi:10.1130/0016-7606(1971)82[2755:Dagoqi]2.0.Co;2

Damuth, J. E., & Fairbridge, R. W. (1970). Equatorial Atlantic Deep-Sea Arkosic Sands and Ice-Age Aridity in Tropical South America. *GSA Bulletin, 81*(1), 189-206. doi:10.1130/0016-7606(1970)81[189:Eadasa]2.0.Co;2

Daneshvar, E., & Worden, R. H. (2017). Feldspar alteration and Fe minerals: origin, distribution and implications for sandstone reservoir quality in estuarine sediments. *Geological Society, London, Special Publications, 435*, SP435. 417.

Dapples, E. C., Krumbein, W. C., & Sloss, L. L. (1953). Petrographic and Lithologic Attributes of Sandstones. *The Journal of Geology, 61*(4), 291-317.

Dickinson, W. R. (1985). Interpreting Provenance Relations from Detrital Modes of Sandstones. In G. G. Zuffa (Ed.), *Provenance of Arenites* (pp. 333-361). Dordrecht: Springer Netherlands.

Dickinson, W. R. (1988). Provenance and sediment dispersal in relation to paleotectonics and paleogeography of sedimentary basins. In *New perspectives in basin analysis* (pp. 3-25): Springer.

Dickinson, W. R., & Suczek, C. A. (1979). Plate-tectonics and sandsone compositions. *Aapg Bulletin-American Association of Petroleum Geologists, 63*(12), 2164-2182.

Dokuz, A., & Tanyolu, E. (2006). Geochemical constraints on the provenance, mineral sorting and subaerial weathering of Lower Jurassic and Upper Cretaceous clastic rocks of the eastern Pontides, Yusufeli (Artvin), NE Turkey. *Turkish Journal of Earth Sciences, 15*(2), 181-209.

Everett, P., Lister, T., Fordyce, F., Ferreira, A., Donald, A., Gowing, C., & Lawley, R. (2019). *Stream sediment geochemical atlas of the United Kingdom*: British Geological Survey.

Folk, R. L. (1956). The role of texture and composition in sandstone classification; discussion. *Journal of Sedimentary Research, 26*(2), 166-171. doi:10.1306/74d70506-2b21-11d7-8648000102c1865d

Folk, R. L. (1968). *Petrology of sedimentary rocks: the University of Texas geology 370K, 383L, 383M*: Austin: Hemphill, 1968.

Folk, R. L. (1980). *Petrology of sedimentary rocks*: Hemphill publishing company.

Griffiths, J., Worden, R. H., Wooldridge, L. J., Utley, J. E. P., Duller, R. A., & Edge, R. L. (2019). Estuarine clay mineral distribution: Modern analogue for ancient sandstone reservoir quality prediction. *Sedimentology*.

Hallam, A. (1975). *Jurassic environments*. Cambridge: Cambridge University Press.

Hallam, A. (1984). Continental humid and arid zones during the jurassic and cretaceous. *Palaeogeography, Palaeoclimatology, Palaeoecology, 47*(3), 195-223. doi:https://doi.org/10.1016/0031-0182(84)90094-4

Hallberg, J. A. (1984). A geochemical aid to igneous rock type identification in deeply weathered terrain. *Journal of Geochemical Exploration, 20*(1), 1-8. doi:https://doi.org/10.1016/0375-6742(84)90085-2

Hansen, D. L., Blundell, D. J., & Nielsen, S. B. (2002). A model for the evolution of the Weald Basin. *Bulletin of the Geological Society of Denmark, 49, Part 2*, 109-118.

Hawkes, P. W., Fraser, A. J., & Einchcomb, C. C. G. (1998). The tectono-stratigraphic development and exploration history of the Weald and Wessex basins, Southern England, UK. *Geological Society, London, Special Publications, 133*(1), 39-65. doi:10.1144/gsl.sp.1998.133.01.03

Herron, M. M. (1986). Mineralogy from Geochemical Well Logging. *Clays and Clay Minerals, 34*(2), 204-213. doi:10.1346/CCMN.1986.0340211

Herron, M. M. (1988). Geochemical classification of terrigenous sands and shales from core or log data. *Journal of Sedimentary Research, 58*(5), 820-829.

Herron, M. M., & Herron, S. L. (1990). Geological applications of geochemical well logging. *Geological Society, London, Special Publications, 48*(1), 165. doi:10.1144/GSL.SP.1990.048.01.14

Hubert, J. F. (1962). A zircon-tourmaline-rutile maturity index and the interdependence of the composition of heavy mineral assemblages with the gross composition and texture of sandstones. *Journal of Sedimentary Research, 32*(3), 440-450. doi:10.1306/74d70ce5-2b21-11d7-8648000102c1865d

Ingersoll, R. (1990). Actualistic sandstone petrofacies: Discriminating modern and ancient source rocks. *Geology, 18*, 733-736. doi:10.1130/0091-7613(1990)018<0733:ASPDMA>2.3.CO;2

Jones, D. K. (Ed.) (1999). *On the uplift and denudation of the Weald* (Vol. 162). London: Geological Society, London, Special Publications.

Kneller, B. C., Scott, R. W., Soper, N. J., Johnson, E. W., & Allen, P. M. (1994). Lithostratigraphy of the Windermere Supergroup, Northern England. *Geological Journal, 29*(3), 219-240. doi:https://doi.org/10.1002/gj.3350290304

Krauskopf, K. (1979). Introduction to Geochemistry, McGraw-Hill Book Co. *New York*.

Krissek, L., & Kyle, P. (2001). Geochemical Indicators of Weathering, Cenozoic Palaeoclimates, and Provenance from Fine-Grained Sediments in CRP-2/2A, Victoria Land Basin, Antarctica. *Terra Antartica, 8*.

Kroonenberg, S. (1992). Effect of provenance, sorting and weathering on the geochemistry of fluvial sands from different tectonic and climatic environments. *Proc. 29th Int. Geol. Congr. Part A. Kyoto, Japan 1992, F. Kumon, K.M. Yu (eds.). VSP Publ., Utrecht (1994) 69-81.*

Lake, S. D., & Karner, G. D. (1987). The structure and evolution of the Wessex Basin, southern England: an example of inversion tectonics. *Tectonophysics, 137*(1), 347-378. doi:https://doi.org/10.1016/0040-1951(87)90328-3

Leeder, M. R., Harris, T., & Kirkby, M. J. (1998). Sediment supply and climate change: implications for basin stratigraphy. *Basin Research, 10*(1), 7-18.

Lowe, D., Sylvester, P., & Enachescu, M. (2011). Provenance and paleodrainage patterns of Upper Jurassic and Lower Cretaceous synrift sandstones in the Flemish Pass Basin, offshore Newfoundland, east coast of Canada. *Aapg Bulletin, 95*, 1295-1320. doi:10.1306/12081010005

Mack, G. H. (2003). Tectonic control of sedimentation. In G. V. Middleton, M. J. Church, M. Coniglio, L. A. Hardie, & F. J. Longstaffe (Eds.), *Encyclopedia of Sediments and Sedimentary Rocks* (pp. 729-734). Dordrecht: Springer Netherlands.

McLimans, R. K., & Videtich, P. E. (1989). Diagenesis and Burial History of Great Oolite Limestone, Southern England1. *AAPG (Am. Assoc. Pet. Geol.) bulletin, 73*(10), 1195-1205. doi:10.1306/44b4aa00-170a-11d7-8645000102c1865d

Middelburg, J. J., van der Weijden, C. H., & Woittiez, J. R. W. (1988). Chemical processes affecting the mobility of major, minor and trace elements during weathering of granitic rocks. *Chemical Geology, 68*(3), 253-273. doi:https://doi.org/10.1016/0009-2541(88)90025-3

Middleton, G. V. (1960). Chemical Composition of Sandstones. *GSA Bulletin, 71*(7), 1011-1026. doi:10.1130/0016-7606(1960)71[1011:Ccos]2.0.Co;2

Milliman, J. D., Summerhayes, C. P., & Barretto, H. T. (1975). Quaternary Sedimentation on the Amazon Continental Margin: A Model. *GSA Bulletin, 86*(5), 610-614. doi:10.1130/0016-7606(1975)86<610:Qsotac>2.0.Co;2

Morad, S., & Adin, A., Ala. (1986). Alteration of detrital Fe-Ti oxides in sedimentary rocks. *GSA Bulletin, 97*(5), 567-578. doi:10.1130/0016-7606(1986)97<567:Aodfoi>2.0.Co;2

Moseley, F. (1978). *The geology of the Lake District*: Yorkshire Geological Society.

Nesbitt, H., Young, G., McLennan, S. M., & Keays, R. (1996). Effects of Chemical Weathering and Sorting on the Petrogenesis of Siliciclastic Sediments, with Implications for Provenance Studies. *The Journal of Geology, 104*, 525-542. doi:10.1086/629850

Nesbitt, H. W., & Young, G. (1982). Early Proterozoic climates and plate motions inferred from major element chemistry of lutites. *Nature, 299*. doi:10.1038/299715a0

Odin, G. S. (1988). *Green Marine Clays: Oolitic Ironstone Facies, Verdine Facies, Glaucony Facies and Celadonite-Bearing Rock Facies-A Comparative Study*. Amsterdam: Elsevier.

Odom, I. E., Doe, T. W., & Dott, R. H. (1976). Nature of feldspar-grain size relations in some quartz-rich sandstones. *Journal of Sedimentary Research, 46*(4), 862-870. doi:10.1306/212f7077-2b24-11d7-8648000102c1865d

Parrish, R. R., Parrish, C. M., & Lasalle, S. (2018). Vein calcite dating reveals Pyrenean orogen as cause of Paleogene deformation in southern England. *Journal of the Geological Society, 175*(3), 425-442. doi:10.1144/jgs2017-107

Pettijohn, F. J., Potter, P. E., & Siever, R. (1973). *Sand and sandstone*. New York: Springer-Verlag.

Pharaoh, T. (2018). The Anglo-Brabant Massif: Persistent but enigmatic palaeo-relief at the heart of western Europe. *Proceedings of the Geologists' Association, 129*(3), 278-328. doi:https://doi.org/10.1016/j.pgeola.2018.02.009

Pirrie, D., Butcher, A. R., Power, M. R., Gottlieb, P., & Miller, G. L. (2004). Rapid quantitative mineral and phase analysis using automated scanning electron microscopy (QemSCAN): Potential applications in forensic geoscience. In K. Pye & D. J. Croft (Eds.), *Forensic Geoscience: Principles, Techniques and Applications* (Vol. 232, pp. 123-136). Bath: Geological Society.

Potter, P. E. (1978). Petrology and Chemistry of Modern Big River Sands. *The Journal of Geology, 86*(4), 423-449.

Radley, J. D. (2006). A Wealden guide; I,; The Weald sub-basin. *Geology Today, 22*(3), 109-118.

Reinson, G. E., Bureau of Mineral Resources, G., & Geophysics. (2015). *Hydrology and sediments of a temperate estuary - Mallacoota Inlet, Victoria*. Retrieved from: http://catalogue.aodn.org.au/geonetwork/srv/eng/metadata.show?uuid=a05f7892-9cfe-7506-e044-00144fdd4fa6, https://researchdata.edu.au/hydrology-sediments-temperate-inlet-victoria

Rider, M. H. (1986). *The geological interpretation of well logs*. United States: John Wiley and Sons, Inc.

Rijkers, R., Duin, E., Dusar, M., & Langenaeker, V. (1993). Crustal structure of the London–Brabant Massif, southern North Sea. *Geological Magazine, 130*, 569-574. doi:10.1017/S0016756800020860

Ruffell, A. H., & Rawson, P. F. (1994). Palaeoclimate control on sequence stratigraphic patterns in the late Jurassic to mid-Cretaceous, with a case study from Eastern England. *Palaeogeography, Palaeoclimatology, Palaeoecology, 110*(1), 43-54. doi:https://doi.org/10.1016/0031-0182(94)90109-0

Sellwood, B. W., Scott, J., & Lunn, G. (1986). Mesozoic basin evolution in Southern England. *Proceedings of the Geologists' Association, 97*(3), 259-289. doi:http://dx.doi.org/10.1016/S0016-7878(86)80020-7

Sellwood, B. W., Scott, J., Mikkelsen, P., & Akroyd, P. (1985). Stratigraphy and sedimentology of the Great Oolite Group in the Humbly Grove Oilfield, Hampshire. *Marine and Petroleum Geology, 2*(1), 44-55. doi:http://dx.doi.org/10.1016/0264-8172(85)90047-9

Sladen, C., & Batten, D. (1984). Source-area environments of Late Jurassic and Early Cretaceous sediments in southeast England. *Proceedings of the Geologists' Association, 95*(2), 149-163.

Taboada, T., Cortizas, A., García, C., & García-Rodeja, E. (2006). Particle-size fractionation of titanium and zirconium during weathering and pedogenesis of granitic rocks in NW Spain. *Geoderma, 131*, 218-236. doi:10.1016/j.geoderma.2005.03.025

Talbot, M. R. (1973). Major sedimentary cycles in the corallian beds (Oxfordian) of Southern England. *Palaeogeography, Palaeoclimatology, Palaeoecology, 14*(4), 293-317. doi:https://doi.org/10.1016/0031-0182(73)90014-X

Tiab, D., & Donaldson, E. C. (2012). *Petrophysics. [electronic book] : theory and practice of measuring reservoir rock and fluid transport properties*: Boston : Gulf Professional Pub./Elsevier, 2012. 3rd ed.

Tobin, R. C., & Schwarzer, D. (2013). Effects of sandstone provenance on reservoir quality preservation in the deep subsurface; experimental modelling of deep-water sand in the Gulf of Mexico. *Special Publication - Geological Society of London, 386*. doi:10.1144/SP386.17

Trueman, S. (2003). The Humbly Grove, Herriard, Storrington, Singleton, Stockbridge, Goodworth, Horndean, Palmers Wood, Bletchingley and Albury Fields, Hampshire, Surrey and Sussex, UK Onshore. In J. G. Gluyas & H. M. Hichens (Eds.), *United Kingdom Oil and Gas Fields Commemorative Millennium Volume* (Vol. 20, pp. 929-941). London: Geological Society, Memoirs.

Tucker, M. E. (1981). *Sedimentary petrology: an introduction* (Vol. 3). Oxford: Blackwell Scientific Publications.

Wentworth, C. K. (1922). A Scale of Grade and Class Terms for Clastic Sediments. *The Journal of Geology, 30*(5), 377-392.

Wooldridge, L. J., Worden, R. H., Griffiths, J., & Utley, J. E. P. (2018). The origin of clay-coated sand grains and sediment heterogeneity in tidal flats. *Sedimentary Geology, 373*, 191-209. doi:10.1016/j.sedgeo.2018.06.004

Worden, R. H., Armitage, P. J., Butcher, A. R., Churchill, J. M., Csoma, A. E., Hollis, C., . . . Omma, J. E. (2018). Petroleum reservoir quality prediction: overview and contrasting approaches from sandstone and carbonate communities. *Geological Society of London Special Publications, 435*, 1. doi:10.1144/sp435.21

Worden, R. H., Griffiths, J., Wooldridge, L. J., Utley, J. E. P., Lawan, A. Y., Muhammed, D. D., . . . Armitage, P. J. (2020). Chlorite in sandstones. *Earth-Science Reviews, 204*, 103105. doi:https://doi.org/10.1016/j.earscirev.2020.103105

Worden, R. H., & Utley, J. (2022). Automated mineralogy (SEM-EDS) approach to sandstone reservoir quality and diagenesis. *Frontiers in Earth Science, 10*, 794266. doi:10.3389/feart.2022.794266

Worden, R. H., Utley, J. E. P., Butcher, A. R., Griffiths, J., Wooldridge, L. J., & Lawan, A. Y. (2018). Improved imaging and analysis of chlorite in reservoirs and modern day analogues: new insights for reservoir quality and provenance. *Geological Society, London, Special Publications, 484*, SP484.410. doi:10.1144/SP484.10

TABLES

Table 1: summary of selected geochemical proxies for lithology, provenance, and weathering.

	Indicator	Elements	Indices (x/x+y)	References
1	Lithology	Si, Al	The Si/(Si+Al) index is a useful indicator of clastic or shale/clay content. A high index is indicative of elevated sand-grade sediment content and the low index is indicative of elevated clay mineral content.	(Herron, 1986; Herron, 1988; Herron & Herron, 1990)
		Fe, K	A high Fe/(Fe+K) index is indicative of elevated Fe-rich clay relative to K-rich clays. In sand-rich sediment, Fe and K oxide ratios have also been applied to differentiate arenaceous and lithic sandstones from arkosic sandstones.	
2	Provenance	Mafic indicators: Ti, Fe, Va, Cr, Ni, Nb, Co, Sc	Clastic sediments with high mafic concentrations are indicative of mafic dominated provenance while elevated felsic concentrations suggest felsic provenance.	(Andersson & Worden, 2004; Bhattacharjee & Mondal, 2021; Krauskopf, 1979)
		Felsic indicators: K, Zr, Si, Th, La, Al		
3	Weathering	K, Al, Zr, Ti, Nb, Ca, Ba, K, Sr and Rb	In general, enrichment in Zr, Al, Ba, and Ti relative to more chemically mobile elements like Ca, Na, K, Rb, and Sr is indicative of chemical weathering.	(Middelburg et al., 1988; Nesbitt et al., 1996; Taboada, Cortizas, García, & García-Rodeja, 2006)

Table 2: Summary of selected QEMSCAN and XRF mineralogy. Both techniques indicate dominant quartz-rich lithology, minor k-feldspar as well as intense weathering characteristics in sand packages PW7-1, PW7-2, PW3-1, PW3-2, BL5-1, BL5-2 and BL5-3.

	Average QEMSCAN fraction		Average XRF proxies		
Sand packages	Quartz (%)	K-feldspar (%)	Sandstone/ shale index (Si/(Si+Al))	K-feldspar chemical weathering index (K/(K+Al))	Zircon mechanical weathering index (Zr/(Zr+Rb))
PW7-1	91.5	1.9	0.961	0.275	0.963
PW7-2	93.7	2.2	0.958	0.272	0.916
PW3-1	96.5	1.7	0.943	0.211	0.835
PW3-2	90.4	2.0	0.964	0.202	0.892
BL5-1	92.8	1.9	0.957	0.304	0.944
BL5-2	82.7	2.4	0.964	0.269	0.925
BL5-3	86.7	4.0	0.963	0.342	0.883

Table 3: Summary of detrital mineralogy for the Corallian sandstones from point counting.

Identifiers		Quartzose grains			Rock fragments					Feldspars			Micas		Fe-rich grains		Bioclast	Apatite	Textural attributes		
Well	Depth (m)	Monocrystalline quartz	Polycrystalline quartz	ΣPoly- + Mono-crystalline quartz	Extra-basinal chert	Extra-basinal quartz-ite	Extra-basinal sand-stone	Extra-basinal mud-stone	Σrock frag-ments	K-feldspar	Plagio-clase	Σfeld-spars	Muscovite	Biotite	Fe-ooids	Glauconite	Bioclast	Apatite	Matrix	Grain size (mm)	Sorting (trask)
PW3	1082.3	22.0	9.0	31.1	0.3	0.3	0.0	0.0	0.6	0.7	0.0	0.7	0.0	0.0	0.3	0.0	3.0	0.3	2.0	0.4	Moderate
PW3	1085.1	33.4	12.8	46.2	0.0	1.0	0.0	0.0	1.0	0.3	0.0	0.3	0.0	0.3	0.6	0.0	0.7	0.3	0.3	0.4	Moderate
PW3	1087.5	35.4	9.7	45.1	0.0	0.0	0.0	0.0	0.0	1.0	0.0	1.0	0.0	0.0	0.0	0.0	1.7	0.0	0.3	0.2	moderate well
PW3	1091.4	38.8	11.7	50.5	0.0	0.7	0.0	0.0	0.7	0.7	0.0	0.7	0.0	0.0	0.0	0.0	0.0	0.3	0.0	0.3	Moderately well
PW3	1091.5	38.5	14.8	53.2	0.0	0.0	0.0	0.0	0.0	0.7	0.0	0.7	0.0	0.0	0.3	0.0	0.0	0.0	0.0	0.3	Moderately well
PW7	1124.0	35.9	15.1	51.0	0.0	0.3	0.0	0.0	0.3	0.0	0.3	0.3	0.0	0.0	0.0	0.0	1.0	0.0	0.0	0.3	Moderately well
PW7	1124.9	35.5	12.4	47.9	0.0	0.0	0.3	0.3	0.6	0.3	0.3	0.6	0.0	0.0	0.0	0.0	0.3	0.0	0.0	0.3	Moderately well
PW7	1126.0	32.9	16.4	49.4	0.0	0.0	0.0	0.0	0.0	0.3	0.3	0.6	0.0	0.0	0.0	0.0	0.9	0.0	0.0	0.3	Moderate
PW7	1130.0	18.1	6.3	24.4	0.0	0.0	0.0	0.0	0.0	0.0	0.0	0.0	0.0	0.0	0.3	0.0	4.6	0.0	0.7	0.4	Moderate
PW7	1131.6	33.5	15.4	48.9	0.0	0.0	0.0	0.0	0.0	0.3	0.0	0.3	0.0	0.0	0.0	0.0	3.4	0.0	0.0	0.3	Moderately well
PW7	1131.7	28.5	11.1	39.6	0.0	0.0	0.0	0.0	0.0	0.7	0.0	0.7	0.0	0.0	0.7	0.0	2.3	0.0	0.0	0.3	Moderately well
PW7	1132.9	33.1	13.4	46.5	0.0	0.3	0.0	0.0	0.3	1.6	0.3	1.9	0.0	0.0	0.0	0.0	0.0	0.0	0.0	0.3	Moderately well
PW7	1133.0	33.1	8.0	41.1	0.3	0.3	0.0	0.0	0.6	0.7	0.0	0.7	0.0	0.0	0.0	0.0	0.7	0.3	0.0	0.3	well
PW7	1134.6	36.5	8.3	44.8	0.0	0.3	0.0	0.0	0.3	2.3	0.3	2.6	0.0	0.3	0.0	0.3	0.3	0.0	18.8	0.2	Moderately well
PW7	1135.2	38.4	14.7	53.2	0.0	1.6	0.0	0.0	1.6	1.0	0.0	1.0	0.0	0.0	0.0	0.0	0.0	0.0	0.0	0.2	Moderately well
BL5	2194.7	41.7	11.4	53.1	0.0	0.0	0.3	0.0	0.3	2.7	0.3	3.0	0.0	0.0	0.0	0.0	1.3	0.3	2.3	0.3	Moderate
BL5	2195.2	38.5	6.3	44.8	0.0	0.0	0.0	0.0	0.0	2.0	0.3	2.3	0.0	0.0	0.0	0.0	0.0	0.0	6.3	0.2	Moderately well
BL5	2197.9	28.7	7.3	36.0	0.0	0.0	0.0	0.0	0.0	2.0	0.0	2.0	0.0	0.0	0.0	0.0	1.0	0.0	13.3	0.2	Moderately well
BL5	2198.8	39.1	6.7	45.8	0.0	0.3	0.0	0.0	0.3	1.3	0.3	1.6	0.0	0.0	0.0	0.3	1.6	0.0	0.0	0.2	Moderate
BL5	2199.1	43.9	10.0	53.9	0.0	0.0	0.0	0.0	0.0	4.0	0.0	4.0	0.0	0.0	0.0	0.7	0.0	0.0	0.3	0.2	Moderate
BL5	2201.9	31.3	10.7	42.0	0.0	0.0	0.0	0.0	0.0	0.3	0.0	0.3	0.0	0.0	0.0	0.0	1.3	1.0	0.0	0.3	Moderately well
BL5	2202.2	37.2	9.3	46.5	0.0	0.7	0.0	0.0	0.7	0.0	0.0	0.0	0.0	0.3	0.0	0.0	0.3	0.0	0.3	0.3	Moderately well
BL5	2204.7	51.5	7.0	58.5	0.0	0.0	0.0	0.0	0.0	1.0	0.3	1.3	0.0	0.0	0.0	0.0	0.6	0.0	0.0	0.2	Moderate
BL5	2205.8	39.0	6.7	45.8	0.0	0.0	0.0	0.0	0.0	2.0	0.0	2.0	0.7	5.0	0.0	0.0	0.7	0.0	4.7	0.2	Moderately well
BL5	2206.6	32.8	3.3	36.1	0.0	0.0	0.0	0.0	0.0	2.7	0.3	3.0	0.3	0.3	0.0	0.3	0.0	0.0	10.0	0.2	Moderate
BL5	2208.0	47.1	5.7	52.9	0.0	1.0	0.0	0.0	1.0	1.0	0.0	1.0	0.0	0.0	0.0	0.0	0.0	0.0	13.4	0.2	Moderate
BL5	2208.9	35.9	4.7	40.6	0.0	0.3	0.0	0.0	0.3	0.7	0.0	0.7	0.0	0.0	0.0	0.0	0.6	0.0	0.0	0.2	Moderately well
BL5	2209.2	53.3	6.7	60.0	0.0	0.3	0.0	0.0	0.3	0.3	0.0	0.3	0.0	0.0	0.0	0.3	0.0	0.0	1.0	0.2	Moderate
BL5	2209.5	52.2	12.4	64.6	0.0	0.0	0.0	0.0	0.0	0.6	0.0	0.6	0.0	0.0	0.0	0.0	1.3	0.0	0.3	0.2	Moderately well
BL5	2210.4	34.8	10.0	44.9	0.0	0.3	0.0	0.0	0.3	0.0	0.3	0.3	0.0	0.0	0.0	0.0	0.0	0.0	2.7	0.2	Moderate
BL5	2211.4	54.6	7.3	62.0	0.0	0.0	0.0	0.0	0.0	0.7	0.0	0.7	0.0	0.0	0.0	0.0	0.9	0.0	0.0	0.2	Moderately well
BL5	2211.5	46.2	15.8	62.0	0.0	0.0	0.0	0.0	0.0	0.0	0.3	0.3	0.0	0.0	0.0	0.0	0.0	0.0	2.9	0.2	Moderate
BL5	2211.6	50.2	10.7	60.9	0.0	0.6	0.0	0.0	0.6	0.3	0.3	0.6	0.0	0.0	0.0	0.0	0.3	0.0	0.0	0.2	Moderate
	Max.	*54.6*	*16.4*	*64.6*	*0.3*	*1.6*	*0.3*	*0.3*	*2.5*	*4.0*	*0.3*	*4.3*	*0.7*	*5.0*	*0.7*	*0.7*	*4.6*	*1.0*	*18.8*	*0.4*	
	Mean	*37.9*	*10.0*	*48.0*	*0.0*	*0.3*	*0.0*	*0.0*	*0.3*	*1.0*	*0.1*	*1.1*	*0.0*	*0.2*	*0.1*	*0.1*	*0.9*	*0.1*	*2.4*	*0.2*	
	Min.	*18.1*	*3.3*	*24.4*	*0.0*	*0.0*	*0.0*	*0.0*	*0.0*	*0.0*	*0.0*	*0.0*	*0.0*	*0.0*	*0.0*	*0.0*	*0.0*	*0.0*	*0.0*	*0.2*	

Table 4: Summary of authigenic mineralogy for the Corallian sandstones from point counting.

Well	Depth (m)	Quartz	Calcite	Dolomite	Siderite	Illite	Kaolinite	Fe-Clay	Pyrite	Apatite
PW3	1082.3	0.0	54.1	0.3	5.0	0.3	0.0	0.0	1.0	1.3
PW3	1085.1	0.0	42.5	0.0	0.3	0.0	0.0	1.0	0.0	0.3
PW3	1087.5	0.0	43.8	0.0	2.2	0.0	0.0	0.0	0.3	0.0
PW3	1091.4	0.0	34.3	0.7	2.3	0.0	0.0	0.3	0.0	0.3
PW3	1091.5	0.3	32.7	0.3	4.0	0.0	0.0	1.5	0.7	0.0
PW7	1124.0	0.0	27.3	0.7	0.3	0.0	0.0	2.2	0.0	0.0
PW7	1124.9	0.0	43.2	0.3	0.0	0.3	0.0	0.3	0.0	0.0
PW7	1126.0	0.0	19.1	1.2	0.0	0.0	0.0	0.3	0.3	0.0
PW7	1130.0	0.0	62.9	0.0	1.2	0.0	0.0	0.3	0.0	0.0
PW7	1131.6	0.3	26.1	0.3	4.6	0.7	0.0	1.5	0.3	0.0
PW7	1131.7	0.0	24.5	1.2	4.3	0.0	0.0	1.6	0.3	0.0
PW7	1132.9	0.0	43.1	0.0	2.3	0.0	0.0	0.0	0.0	0.0
PW7	1133.0	0.0	51.8	0.0	0.6	0.9	0.0	0.0	0.3	0.3
PW7	1134.6	0.0	5.9	0.7	2.0	8.3	1.0	1.0	1.0	0.0
PW7	1135.2	0.0	39.4	0.0	0.3	0.0	0.0	0.0	0.3	0.0
BL5	2194.7	0.7	24.9	7.1	0.3	2.3	0.0	0.7	2.0	0.6
BL5	2195.2	1.3	37.8	1.0	1.3	1.3	0.3	0.0	1.3	0.0
BL5	2197.9	0.7	22.4	17.7	2.0	0.3	0.0	0.0	2.7	0.0
BL5	2198.8	0.0	42.0	2.1	0.6	2.0	0.0	0.7	1.7	0.0
BL5	2199.1	7.9	6.4	1.0	0.3	0.7	0.3	2.5	1.7	0.0
BL5	2201.9	0.0	48.8	0.0	0.9	0.0	0.0	0.6	0.3	1.0
BL5	2202.2	0.3	39.4	1.3	1.7	0.3	0.0	1.4	0.0	0.0
BL5	2204.7	0.7	10.2	1.0	1.0	2.7	0.0	3.6	1.0	0.0
BL5	2205.8	1.0	6.3	0.7	0.7	22.3	0.3	1.3	0.7	0.0
BL5	2206.6	0.7	22.4	8.3	1.7	12.0	0.0	1.3	0.6	0.0
BL5	2208.0	0.7	3.0	0.3	0.7	10.6	0.0	0.6	1.0	0.0
BL5	2208.9	0.0	46.0	0.9	0.7	2.6	0.0	1.6	0.3	0.0
BL5	2209.2	0.3	16.0	0.0	0.0	3.9	0.3	1.0	0.0	0.0
BL5	2209.5	0.0	9.2	0.7	0.0	1.0	0.0	1.0	0.0	0.0
BL5	2210.4	0.0	38.7	0.3	1.3	1.0	0.3	0.0	1.0	0.0
BL5	2211.4	3.0	1.9	1.3	0.3	2.3	0.0	1.3	1.6	0.0
BL5	2211.6	0.6	9.0	2.7	0.7	2.0	0.3	0.3	0.0	0.0
BL5	2211.6	2.0	7.3	0.3	0.0	1.7	0.3	2.3	0.7	0.0
	Max.	*7.9*	*62.9*	*17.7*	*5.0*	*22.3*	*1.0*	*3.6*	*2.7*	*1.3*
	Mean	*0.6*	*29.2*	*1.6*	*1.4*	*2.4*	*0.1*	*0.9*	*0.6*	*0.1*
	Min.	*0.0*	*1.9*	*0.0*	*0.0*	*0.0*	*0.0*	*0.0*	*0.0*	*0.0*

FIGURES

FIGURE 1. Geological map of the Weald Basin showing surface geology major structural trends as well as the London-Brabant Massif. (a) Shows the location of the Palmers Wood and Bletchingley fields which are separated by a fault to the north of the Weald Basin. (b) Schematic cross-section of (a) showing faults and subsurface geologic units. (c) Palaeogeographic map of Upper Oxfordian areas of southern England after Brookfield (1973) showing some facies distribution in areas including the Weald Basin and London-Brabant Massif to the south up to the Pennine Massif in the north.

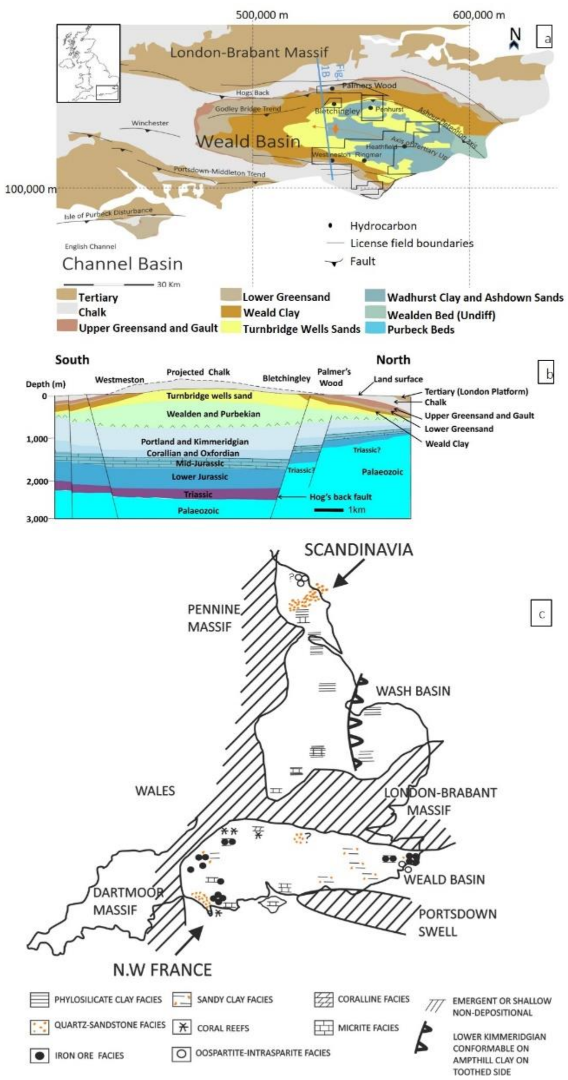

FIGURE 2. Generalised stratigraphic section for the Jurassic of the Weald Basin as modified from Trueman (2003). The Corallian Sandstone Formation is highlighted in brown.

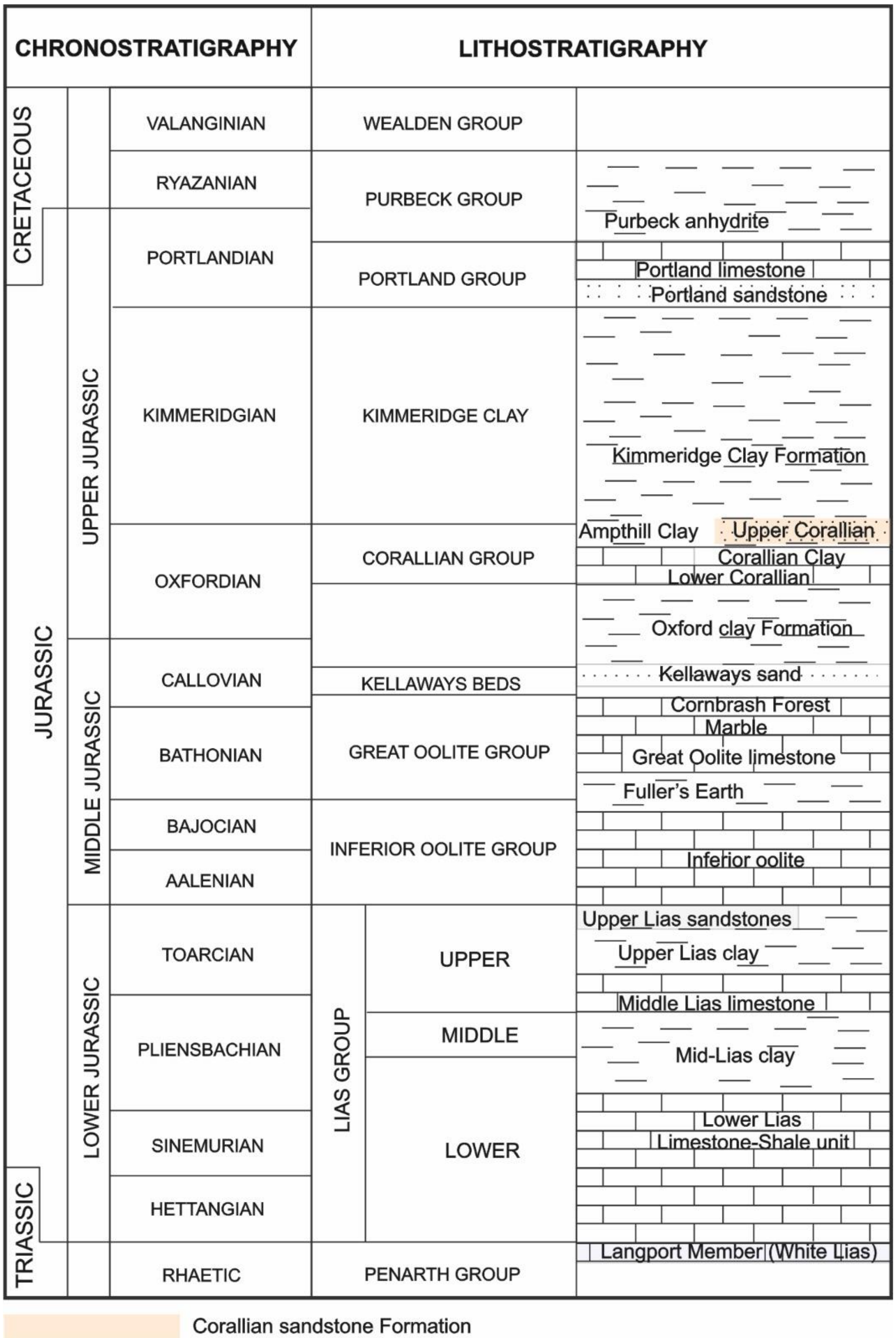

FIGURE 3. shows sedimentary logs from PW7 (a) PW3 (b) and BL5 (c). The sedimentary logs show the lithology and sedimentary structures in the Corallian sandstones. The NPHI_RHOB (neutron porosity and bulk density) cross-over plots separate the sand-rich from the clay-rich sections of the sedimentary logs. The sand-rich sections are labelled by well as PW7-1, PW7-2, PW3-1, PW3-2, BL5-1, BL5-2 and BL5-3. Lithostratigraphic correlation show that none of the sand packages correlate with sand package BL5-3 which suggests that BL5-3 has a different genetic relationship to the other sand packages.

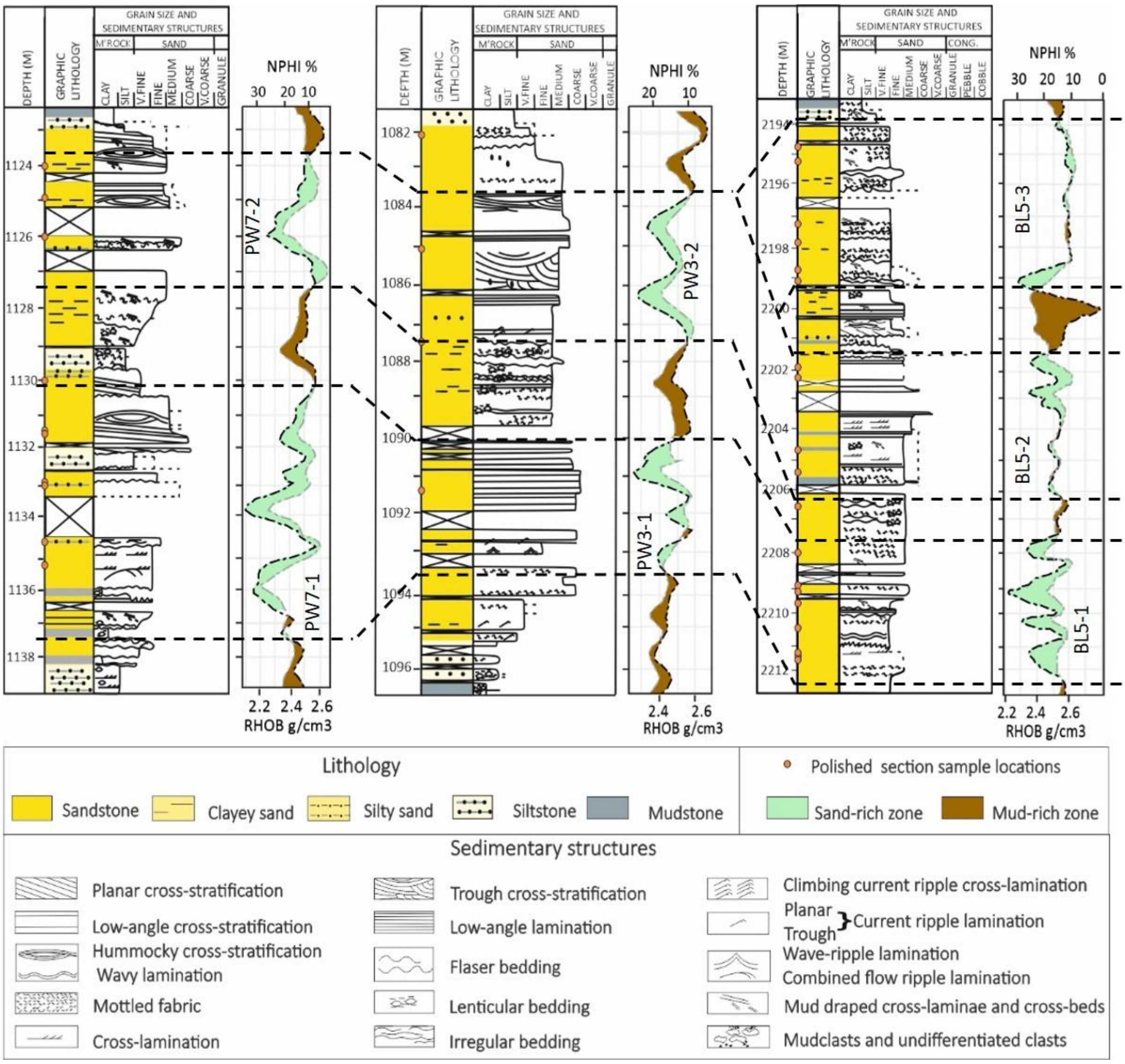

FIGURE 4. shows proxies for provenance, bulk lithology, mineralogy and weathering in the Corallian sandstones. The elements are expressed in atomic fractions to discount for quartz dilution and vector points have been included for granite and basalt using molar proportions calculated from Krauskopf (1979). (a) Compares Ti and Al content as proxies for mafic vs. felsic provenance. Sample points plot between the basalt and granite lines to indicate a source-area lithology of mixed mafic-felsic (intermediate) composition. Sample points cluster close to the origin to suggest hydrologic enrichment of quartz. (b) Sample points plot predominantly away from the basalt and granite line and cluster closer to the quartz line to underscore vast quartz enrichment by hydrologic processes. (c) Vast sample points cluster around the graph's origin to indicate hydrologic enrichment of quartz. The elevated Al content is indicative of intense weathering. (d) Reflects local Fe enrichment in the sediments. The samples that plot away from the granite and basalt lines suggest Fe-enrichment by secondary processes such as weathering and diagenesis. (e) The Ti-Fe plot shows many sample points clustered along the basalt and granite lines to indicate significant mafic input to the sediments regardless of protolith. The plot indicates elevated Fe-rich rather than Ti-rich mafic influence on the sediments. (f) Is a proxy for weathering with elevated Zr as well as the clustering of sample points at the origin indicates enrichment of quartz by intense weathering.

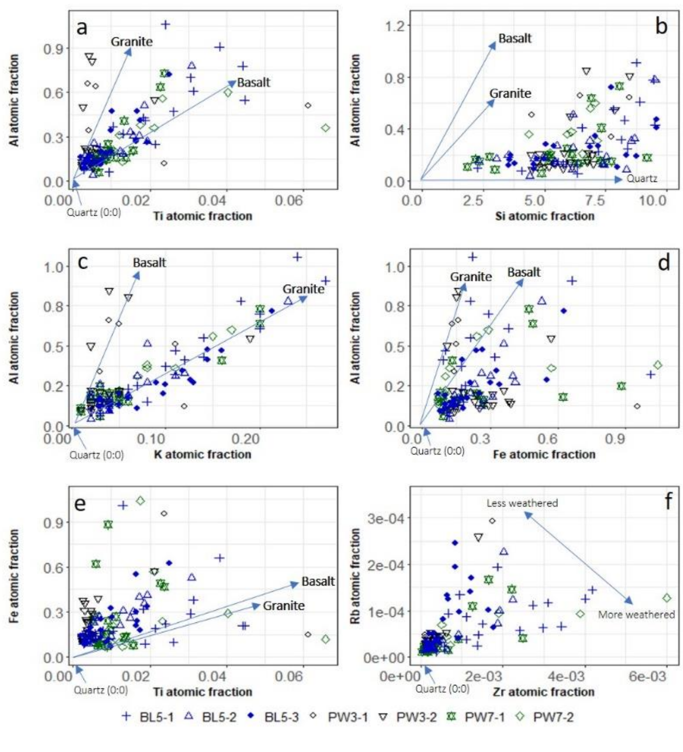

FIGURE 5. Box plots show selected element indices by sand packages calculated using their ppm concentration. The grey lines in the boxes are the mean values for each well. (a) shows high silica index for all sand packages indicative of vast quartz enrichment due to hydrological sorting. (b) indicates elevated Al content due to intense weathering in the sand packages similar to the chemical index of alteration of Nesbitt and Young (1982). BL5-1, 2 and 3 have elevated K values which suggests less intense weathering in the Bletchingley area (c) also emphasizes intense weathering by the enrichment of the more resistant Zr relative to the more mobile Rb (d) shows differential sedimentological Fe-enrichment in the sand packages (e) the Ti-Al index shows dominant intermediate mean values between the mafic and felsic lines. The mafic and felsic lines are drawn based on ppm concentration of elements in basalt and granite respectively as reported in Krauskopf (1979).

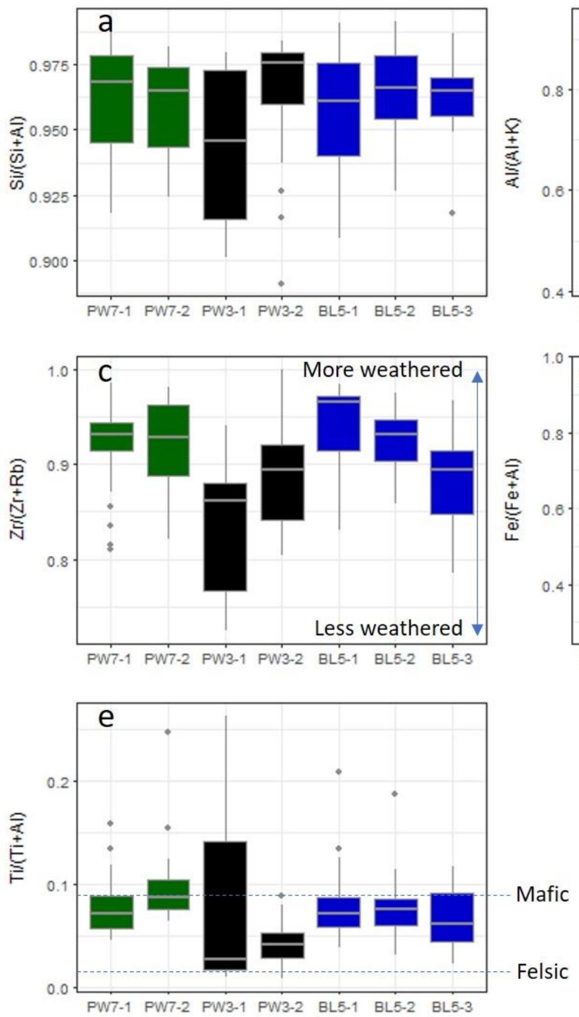

FIGURE 6. shows petrographic images which highlight the main mineralogy in the Corallian sandstones. (a) Is a cross-polarised image from PW3 (1083.1 m) highlighting monocrystalline and polycrystalline quartz, calcite cement, pyrite cement and a bivalve bioclast. The monocrystalline quartz at the top centre-left shows undulose extinction typical of metamorphic quartz. (b) Is from PW7 (1131.9 m) showing pervasive calcite cement and several bivalve bioclasts under different stages of neomorphism and/or dissolution to form calcite cement. (c) Is from BL5_ (2199.92 m), it shows pervasive siderite matrix in a fine- to medium-grained sandstone. (d) Is from PW7 (1138.04 m), it shows detrital matrix draped over a fine-grained sandstone. Abbreviations: Qtz: quartz, mqtz: monocrystalline quartz, pqtz: polycrystalline quartz, Eqtz: embayed quartz; cal: calcite, py: pyrite, ksp: K-feldspar, dol: dolomite, brt: berthierine, bi: bivalve. Optical petrography suggests a felsic origin with potential significant sediment transport or reworking before deposition. The occurrence of iron-rich minerals also suggests significant input of iron from the source-area or sedimentological Fe-enrichment.

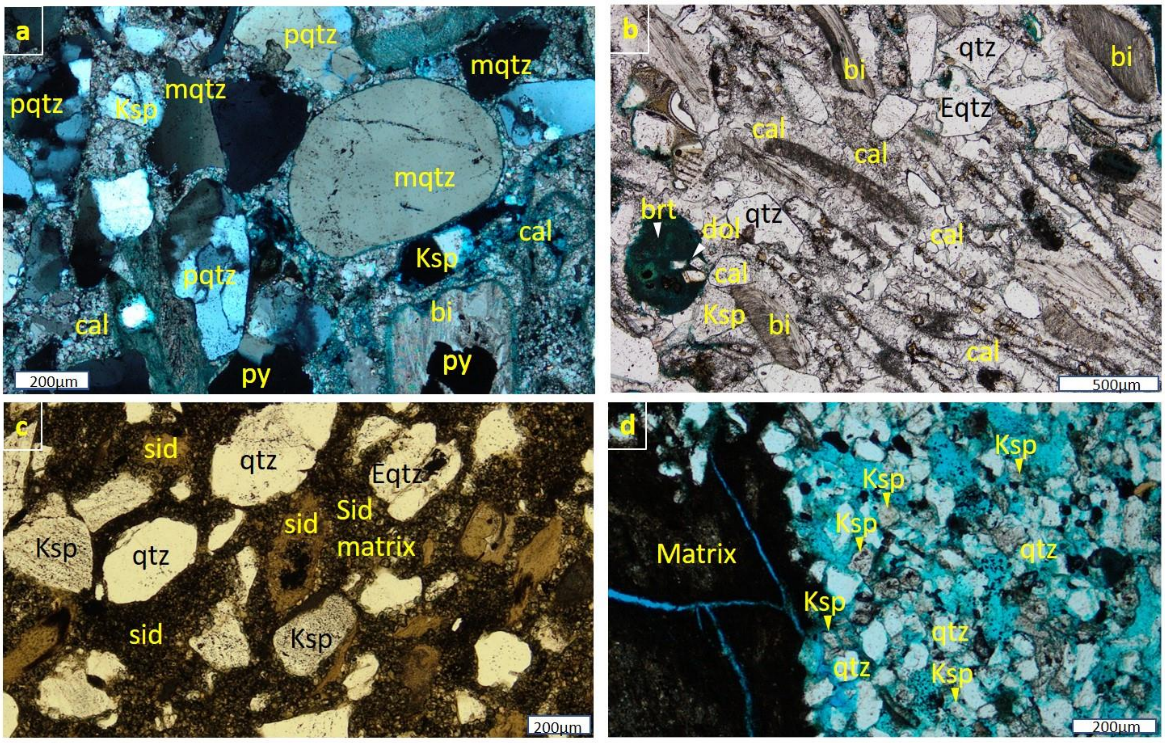

FIGURE 7. QEMSCAN images from (a) PW7 (1132.88 m) showing pervasive calcite and siderite cementation in fine-grained sand. (b) BL5 (2199.92 m) shows pervasive siderite matrix on the top-right to center field of view and authigenic berthierine at the bottom-left to center field of view. (c) Shows intense cementation by Fe-rich minerals Fe-dolomite, and pyrite. (d) Is a QEMSCAN image from PW7 (1124.3 m) which highlights the diverse mineralogy in the detrital clays as well as shows authigenic dolomite, Fe-dolomite and calcite.

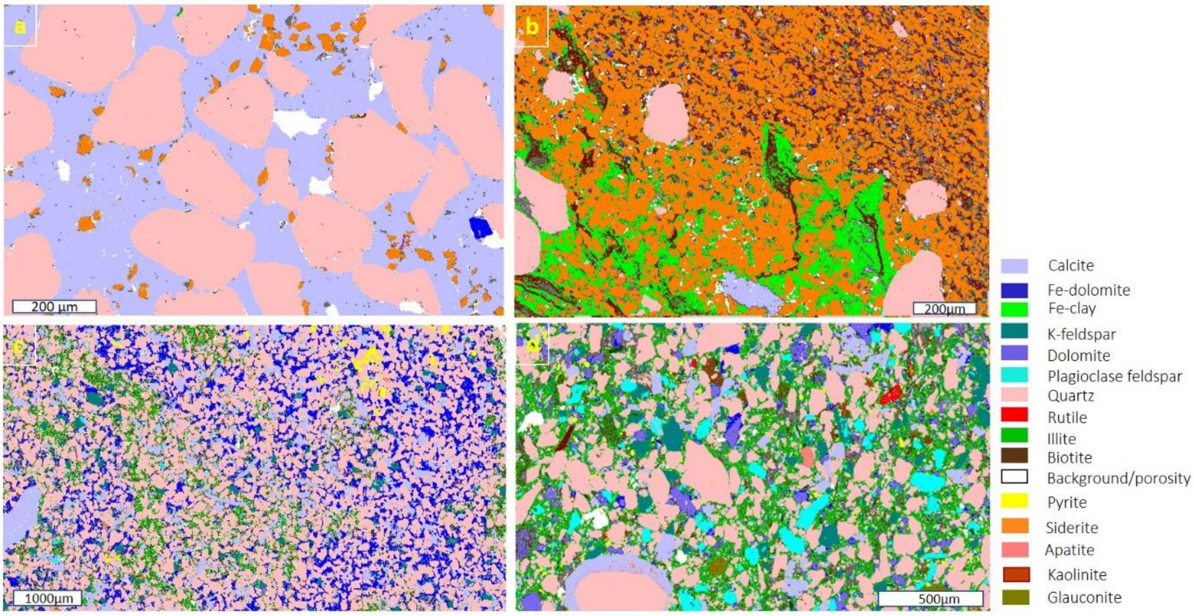

FIGURE 8. SEM-EDS micrographs showing mineralogy of the Corallian sandstones. (a) Shows slightly altered K-feldspar, siderite, kaolinite, pyrite, dolomite and quartz. (b) Shows a berthierine ooid in calcite cement. The ooid is held in the rock fabric by calcite cement, typical of detrital grains. (c) Shows embayed quartz in a calcite-cemented rock. Abbreviations: py: pyrite, k-fsp: potassium feldspar, qtz: quartz, Eqtz: embayed quartz; dol: dolomite, ka: kaolinite, brt: berthierine.

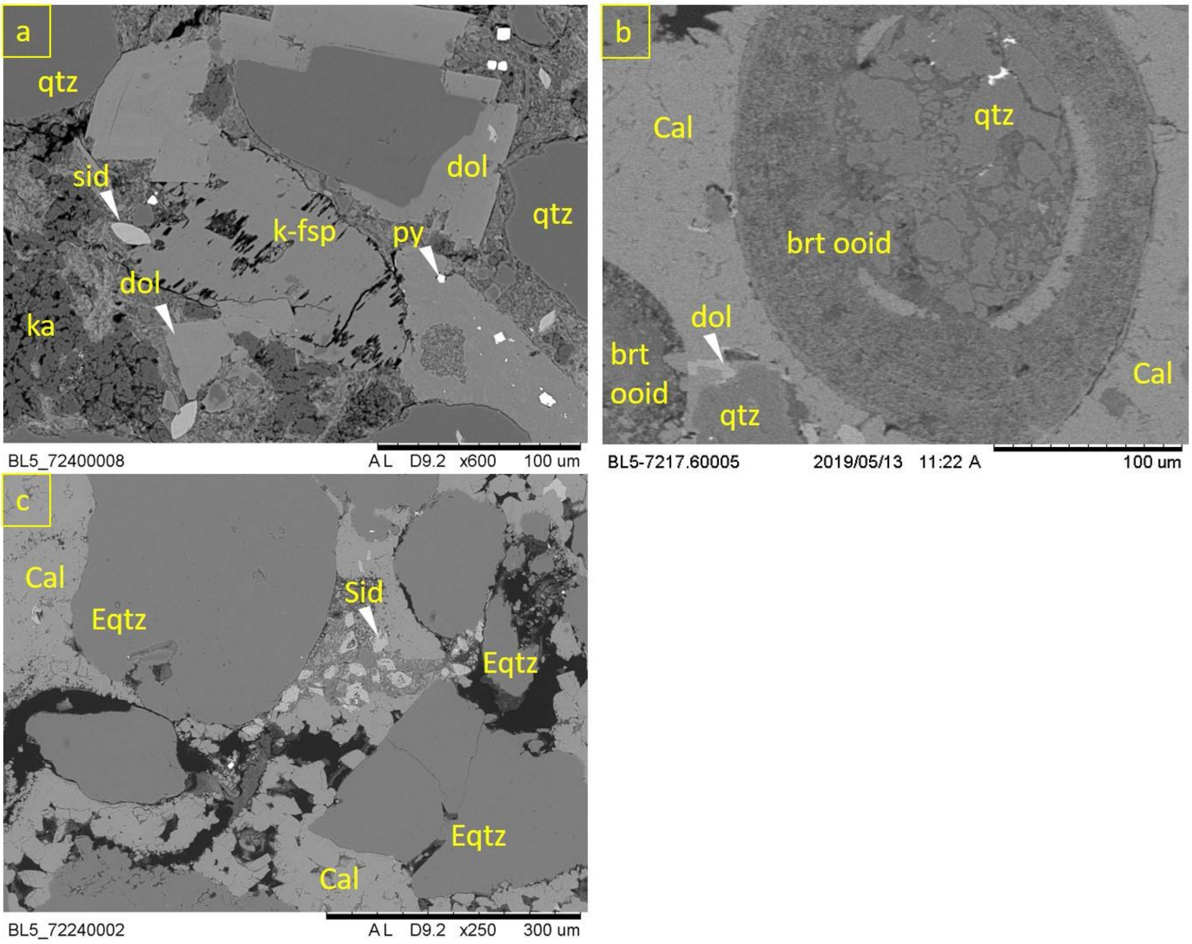

FIGURE 9. (a) QtFL plot for PW7, PW3 and BL5 showing the relative proportion in percent of total detrital quartz (Qt), feldspars (F), and lithic grains (L). The plot shows a dominant quartz-rich lithology for the sandstones with minor feldspars and lithic grain fragments. This is indicative of a mature sediment source typical of long sediment transport and/or reworked sediments which has undergone intense hydrologic sorting. (b) QmFL compositional plot of the Corallian sandstones: (after Dickinson, 1985) to show source-area tectonic setting. Monocrystalline quartz shows a dominant proportion above 60% relative to feldspars and lithic grain components (Igneous +sedimentary +metamorphic rock fragments). The sample points plot dominantly in the quartzose recycled orogen region with BL5 having more monocrystalline quartz than PW3 and PW7. Sandstone package BL5-3 has more feldspars and clusters close to the craton interior orogen. (c) The lithic fragments plot dominantly in the metamorphic zone (>90%) with minor sedimentary clasts (<5%) and no igneous grains. The dominance of quartzose sediments and low feldspar content suggests an intensely weathered hinterland.

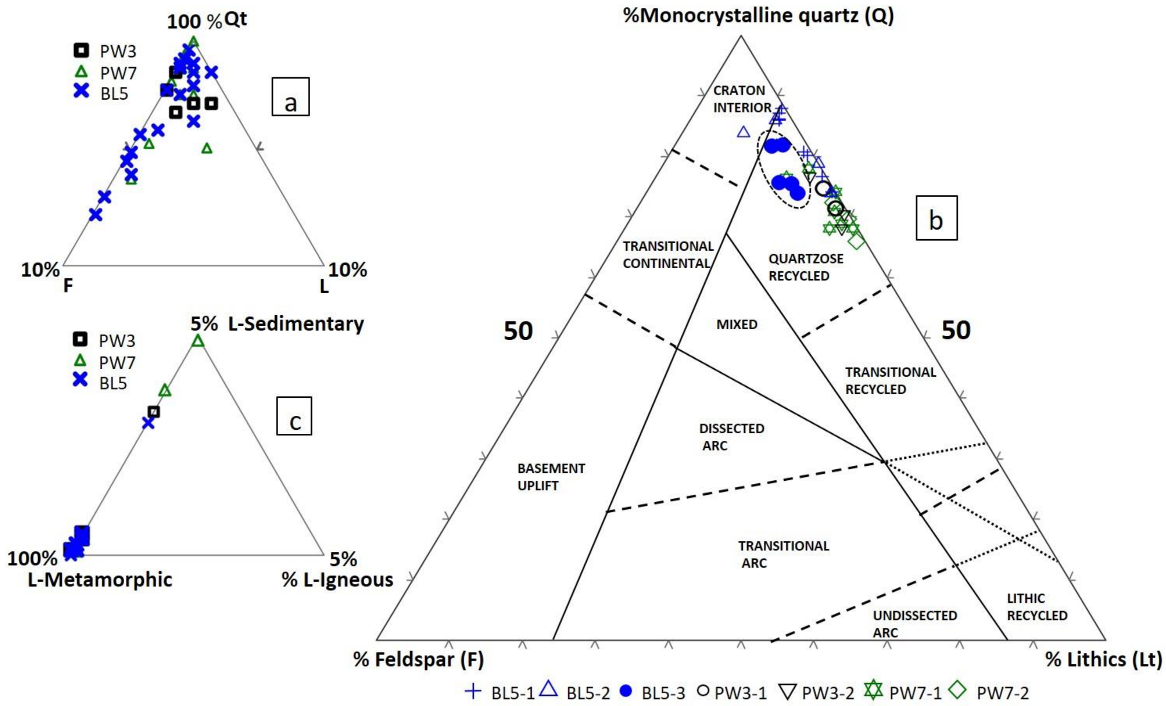

FIGURE 10. Boxplots for selected point count data for the Corallian sandstones (a) shows box plots for grain size measured from point counting analysis with grain sizes highlighted according to the Wentworth (1922) scale. The plots show medium-grained fractions in PW7-1 to PW3-2 and finer-grained fractions in BL5-1 to BL5-3 (b) shows more monocrystalline quartz in BL5-1 to BL5-3 with the highest occurrence in BL5-1 (c) shows less polycrystalline quartz in BL5-1 to BL5-3.

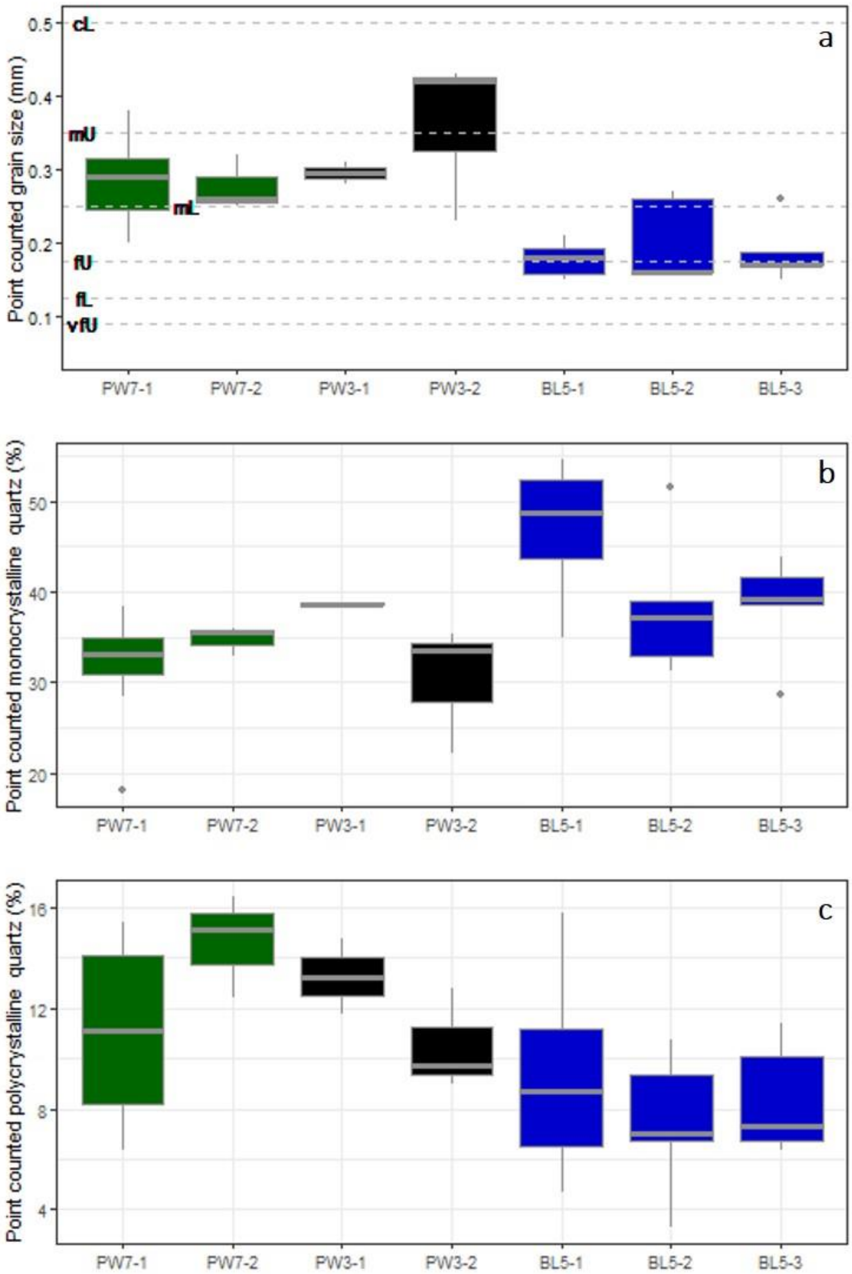

FIGURE 11. Boxplots of SEM-EDS mineralogy for the Corallian sandstones as a function of sand packages. The plots have been normalised for porosity, bioclasts and diagenetic components: calcite, siderite, dolomite, Fe-dolomite and pyrite with the detrital grain percentages expressed in the boxplots. (a) Shows high quartz content from ~65% to ~97% with sand packages BL5-2 and BL5-3 having the least sand content. (b) and (c) show K-feldspar and plagioclase feldspar, respectively with BL5-2 and BL5-3 showing the highest feldspar content. (d) Shows trace amounts of zircon in PW7-1 to PW3-1 with increase in PW3-2 and the highest content in BL5-1, BL5-2 and BL5-3. Rutile shows varied levels in the sand packages with BL5-1, BL5-2 and BL5-3 showing the highest quantity of rutile. (e). Illite (f) and muscovite (g) shows the highest content in BL5-2 with lesser content in BL5-3, BL5-1, PW3-2 and PW7-1, PW7-2 and PW3-1 having trace quantities. (h) Biotite has the highest content in BL5-2, similar to Fe-clay (i) and kaolinite (j). The mineralogical differences in BL5 suggests either a source-area evolution or tectonic controls on sediment distribution and transportation.